NATIONAL ADVISORY COMMITTEE FOR AERONAUTICS

REPORT No. 829

SUMMARY OF MEASUREMENTS IN LANGLEY FULL-SCALE TUNNEL OF MAXIMUM LIFT COEFFICIENTS AND STALLING CHARACTERISTICS OF AIRPLANES

By HAROLD H. SWEBERG and RICHARD C. DINGELDEIN

1945

For sale by the Superintendent of Documents, U. S. Government Printing Office, Washington 25, D. C. - - - - - Price 25 cents

AERONAUTIC SYMBOLS

1. FUNDAMENTAL AND DERIVED UNITS

	Symbol	Metric		English	
		Unit	Abbreviation	Unit	Abbreviation
Length	l	meter	m	foot (or mile)	ft (or mi)
Time	t	second	s	second (or hour)	sec (or hr)
Force	F	weight of 1 kilogram	kg	weight of 1 pound	lb
Power	P	horsepower (metric)		horsepower	hp
Speed	V	kilometers per hour	kph	miles per hour	mph
		meters per second	mps	feet per second	fps

2. GENERAL SYMBOLS

W Weight$=mg$

g Standard acceleration of gravity$=9.80665$ m/s^2 or 32.1740 ft/sec^2

m Mass$=\frac{W}{g}$

I Moment of inertia$=mk^2$. (Indicate axis of radius of gyration k by proper subscript.)

μ Coefficient of viscosity

ν Kinematic viscosity

ρ Density (mass per unit volume)

Standard density of dry air, 0.12497 kg-m^{-4}-s^2 at 15° C and 760 mm; or 0.002378 lb-ft^{-4} sec^2

Specific weight of "standard" air, 1.2255 kg/m^3 or 0.07651 lb/cu ft

3. AERODYNAMIC SYMBOLS

S Area

S_w Area of wing

G Gap

b Span

c Chord

A Aspect ratio, $\frac{b^2}{S}$

V True air speed

q Dynamic pressure, $\frac{1}{2}\rho V^2$

L Lift, absolute coefficient $C_L=\frac{L}{qS}$

D Drag, absolute coefficient $C_D=\frac{D}{qS}$

D_0 Profile drag, absolute coefficient $C_{D_0}=\frac{D_0}{qS}$

D_i Induced drag, absolute coefficient $C_{D_i}=\frac{D_i}{qS}$

D_p Parasite drag, absolute coefficient $C_{D_p}=\frac{D_p}{qS}$

C Cross-wind force, absolute coefficient $C_C=\frac{C}{qS}$

i_w Angle of setting of wings (relative to thrust line)

i_t Angle of stabilizer setting (relative to thrust line)

Q Resultant moment

Ω Resultant angular velocity

R Reynolds number, $\rho\frac{Vl}{\mu}$ where l is a linear dimension (e.g., for an airfoil of 1.0 ft chord, 100 mph, standard pressure at 15° C, the corresponding Reynolds number is 935,400; or for an airfoil of 1.0 m chord, 100 mps, the corresponding Reynolds number is 6,865,000)

α Angle of attack

ϵ Angle of downwash

α_0 Angle of attack, infinite aspect ratio

α_i Angle of attack, induced

α_a Angle of attack, absolute (measured from zero-lift position)

γ Flight-path angle

REPORT No. 829

SUMMARY OF MEASUREMENTS IN LANGLEY FULL-SCALE TUNNEL OF MAXIMUM LIFT COEFFICIENTS AND STALLING CHARACTERISTICS OF AIRPLANES

By HAROLD H. SWEBERG and RICHARD C. DINGELDEIN

Langley Memorial Aeronautical Laboratory
Langley Field, Va.

National Advisory Committee for Aeronautics

Headquarters, 1500 New Hampshire Avenue NW., Washington 25, D. C.

Created by act of Congress approved March 3, 1915, for the supervision and direction of the scientific study of the problems of flight (U. S. Code, title 49, sec. 241). Its membership was increased to 15 by act approved March 2, 1929. The members are appointed by the President, and serve as such without compensation.

TECHNICAL COMMITTEES

AERODYNAMICS

POWER PLANTS FOR AIRCRAFT

AIRCRAFT CONSTRUCTION

OPERATING PROBLEMS

MATERIALS RESEARCH COORDINATION

Coordination of Research Needs of Military and Civil Aviation

Preparation of Research Programs

Allocation of Problems

Prevention of Duplication

LANGLEY MEMORIAL AERONAUTICAL LABORATORY
Langley Field, Va.

AMES AERONAUTICAL LABORATORY
Moffett Field, Calif.

AIRCRAFT ENGINE RESEARCH LABORATORY, Cleveland Airport, Cleveland, Ohio

Conduct, under unified control, for all agencies, of scientific research on the fundamental problems of flight

---

OFFICE OF AERONAUTICAL INTELLIGENCE, Washington, D. C.

Collection, classification, compilation, and dissemination of scientific and technical information on aeronautics

REPORT NO. 829

SUMMARY OF MEASUREMENTS IN LANGLEY FULL-SCALE TUNNEL OF MAXIMUM LIFT COEFFICIENTS AND STALLING CHARACTERISTICS OF AIRPLANES

By Harold H. Sweberg and Richard C. Dingeldein

SUMMARY

The results of measurements in the Langley full-scale tunnel of the maximum lift coefficients and stalling characteristics of airplanes have been collected. The data have been analyzed to show the nature of the effects on maximum lift and stall of wing geometry, fuselages and nacelles, propeller slipstream, surface roughness, and wing leading-edge appendages such as ducts, armaments, tip slats, and airspeed heads. Comparisons of full-scale-tunnel and flight measurements of maximum lift and stall are included in some cases and the effects of the different testing techniques on the maximum-lift measurements are also given.

The results indicated that large improvements in the maximum lift and stalling characteristics of airplanes can be obtained by careful attention to detail design. Surface roughness, wing leakage, and the improper location of ducts, armament, and slats at the leading edge of a wing have been found to cause serious losses in the maximum lift coefficient of an airplane. Wings having high taper ratios and large amounts of sweepback have been shown to be subject to poor stalling characteristics because they are susceptible to tip stalling. The proper combinations of washout and changes in camber and wing thickness from root to tip with taper will usually produce satisfactory stalls on wings subject to tip stalling. A comparison of full-scale-tunnel and flight measurements of the maximum lift coefficient of an airplane showed that satisfactory agreement may be obtained if the comparison is made under similar test conditions, such as Reynolds number, slipstream, and time rate of change of angle of attack.

INTRODUCTION

A considerable amount of data have been obtained relative to the maximum lift coefficients and the stalling characteristics of the military airplanes and mock-ups tested in the Langley full-scale tunnel. The results of these tests, which have been reported separately, have been incorporated in the present report to facilitate the use of the data by airplane designers.

The data include, mainly, lift curves and tuft surveys for each airplane in the service condition and as modified in various ways in attempts to improve the maximum lift and the stalling characteristics. The effects of wing geometry, such as taper and sweep, are shown with the effects of propeller operation, Reynolds number, and other characteristics of the testing techniques. The effects on maximum lift and stall of adding irregularities, such as nacelles, guns, cooling ducts, and airspeed heads, to the wing surfaces are also shown. Flight observations of the stall were available for some of the airplanes and have been included in the discussion with an analysis of the differences between wind-tunnel and flight results. The increments of lift coefficient due to split and slotted flaps as calculated from the results of tests in two-dimensional flow are compared with the increments obtained from these flaps when installed on the airplanes.

AIRPLANES AND EQUIPMENT

Pertinent descriptive data for the airplanes tested are given in table I and in the three-view drawings of figure 1. Photographs of the airplanes and mock-ups mounted in the Langley full-scale tunnel are presented as figure 2. Most of the airplanes and mock-ups are shown in the condition as received at the Langley full-scale tunnel (designated service condition); a few are shown in various stages of modification as described in figure 2.

The Langley full-scale tunnel and its equipment are described in reference 1.

METHODS AND TESTS

The stall was investigated by noting the behavior of numerous wool tufts, approximately 3 inches long, attached to the upper wing surfaces of the airplanes. Violent fluctuations and reversals of the flow direction of the tufts indicated separation of the air flow from the wing surface. In some instances the tufts were attached, at various heights above the wing surfaces, to light masts in order to obtain a more positive indication of separation. The use of masts was found to be particularly desirable on wings having low-drag airfoil sections and large amounts of sweepback since, in these cases, the boundary-layer flow caused the surface tufts to change direction and appear stalled before actual separation occurred.

The behavior of the tufts was studied over a range of angle of attack above and below the angle of maximum lift. For several of the airplanes, observations were made with the landing flaps retracted and deflected and with the propellers removed and operating at various thrust coefficients. In each case, force measurements were made of the variation of lift with angle of attack to supplement visual and photographic observations of the wool tufts. The angles of attack shown in the figures refer, in every case, to the angle of the wing root chord line with the free-stream direction.

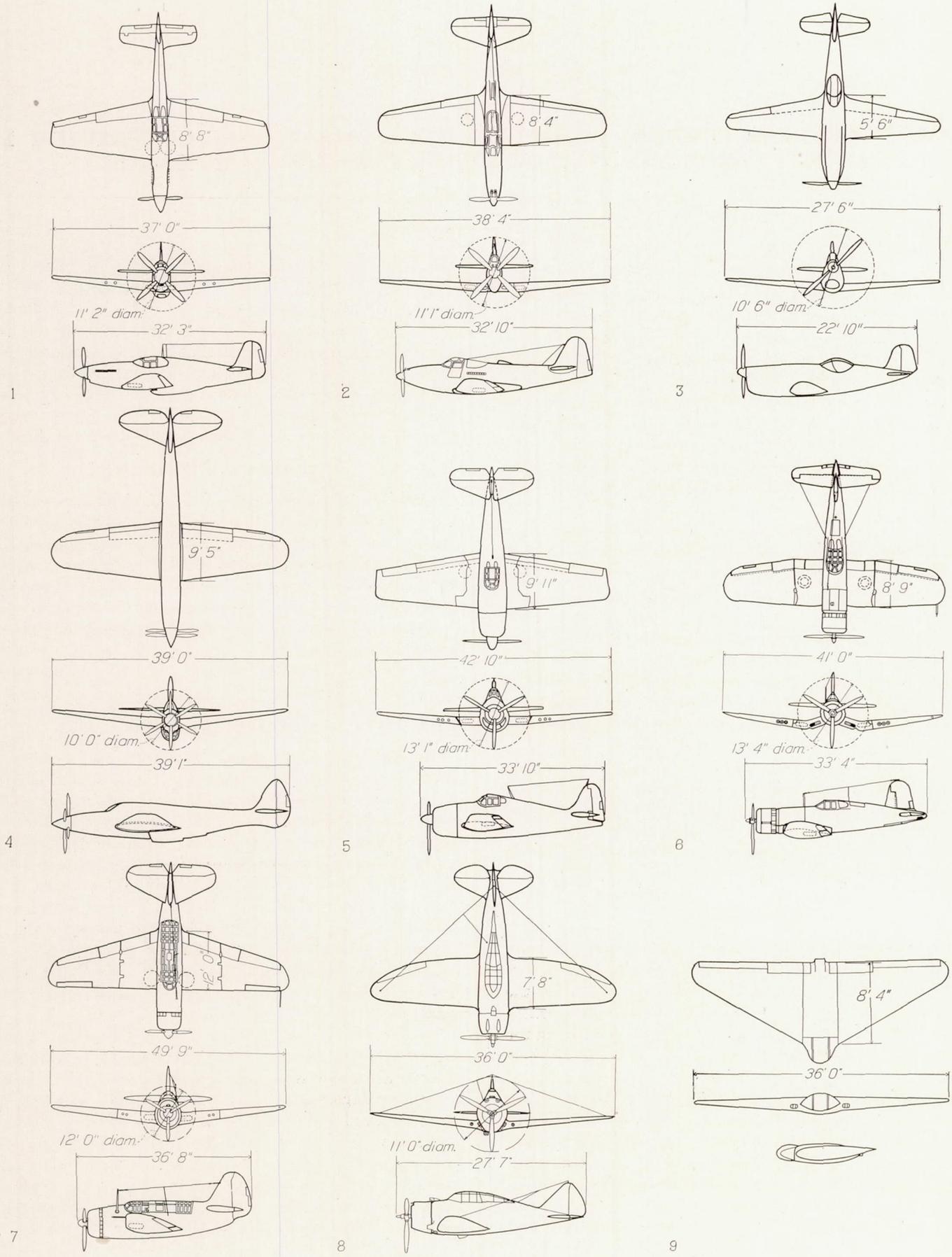

FIGURE 1.—Airplanes and mock-ups.

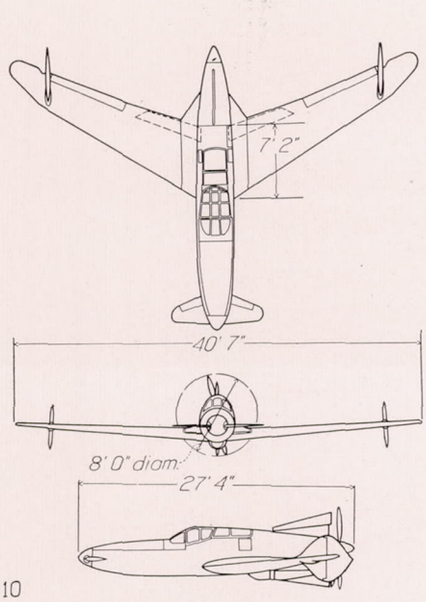

10

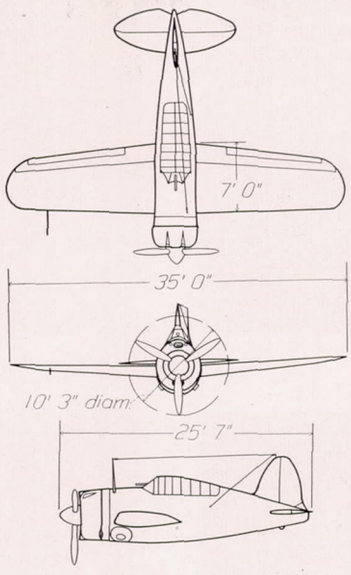

11

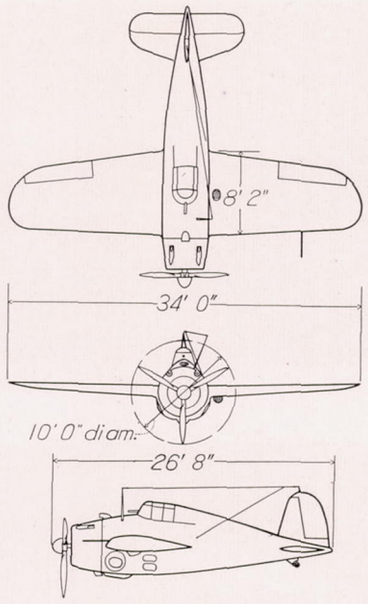

12

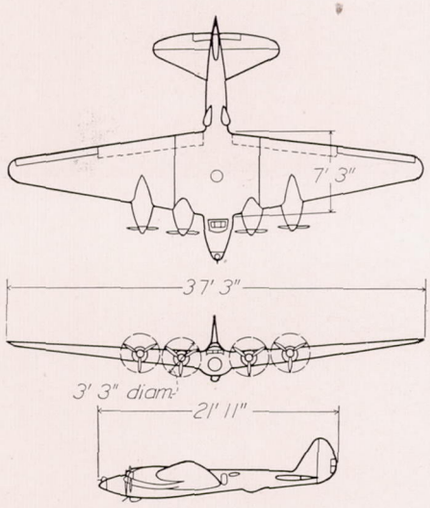

13

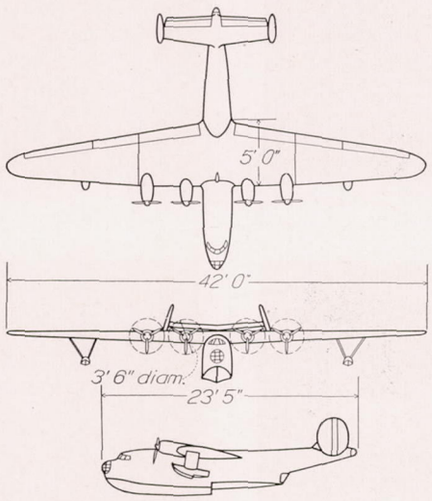

14

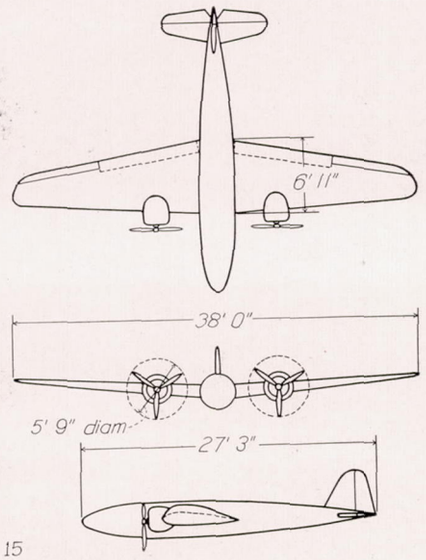

15

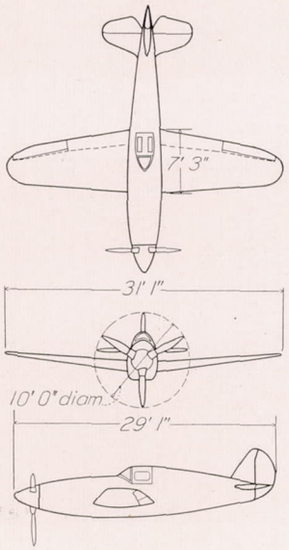

16

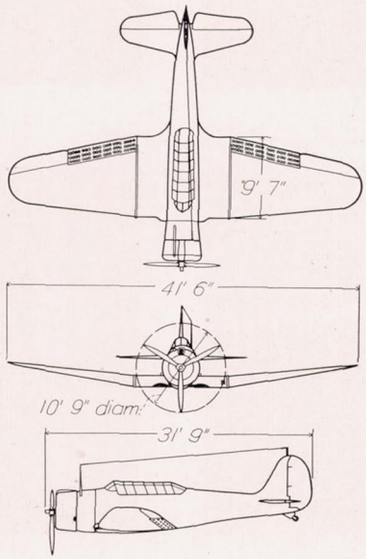

17

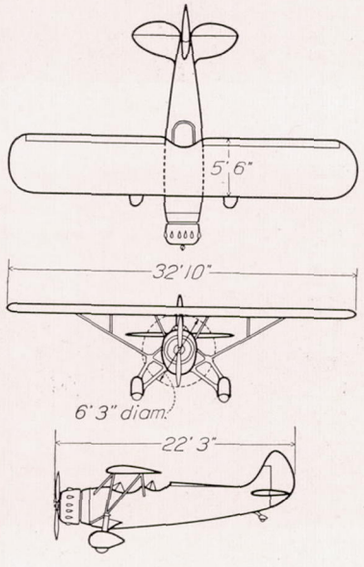

18

FIGURE 1.—Concluded.

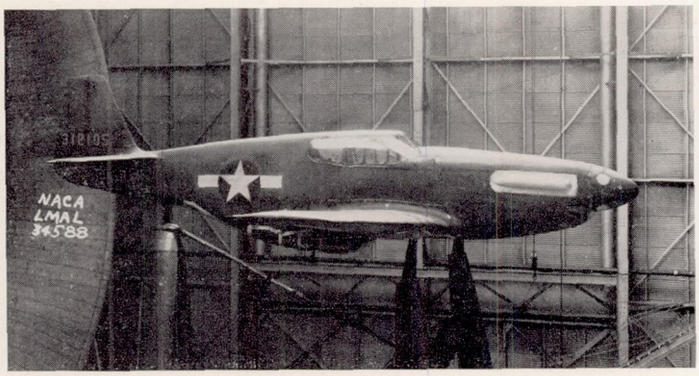

(a) Airplane 1 in faired and sealed condition.

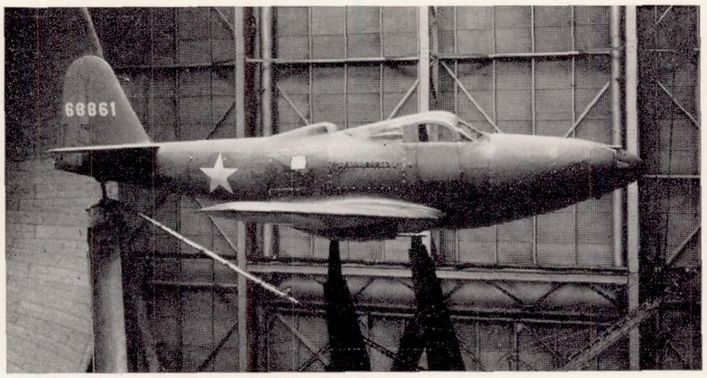

(b) Airplane 2 in service condition.

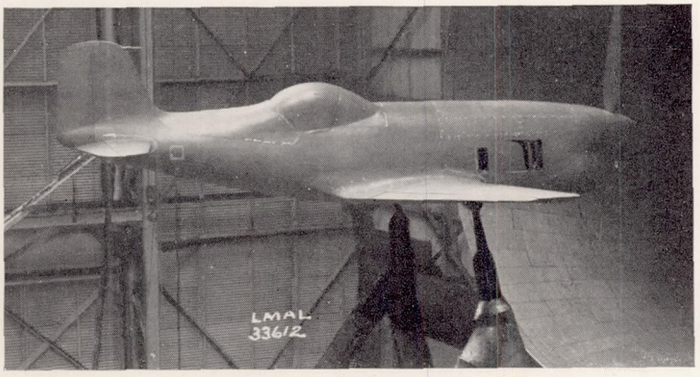

(c) Airplane 3; complete mock-up.

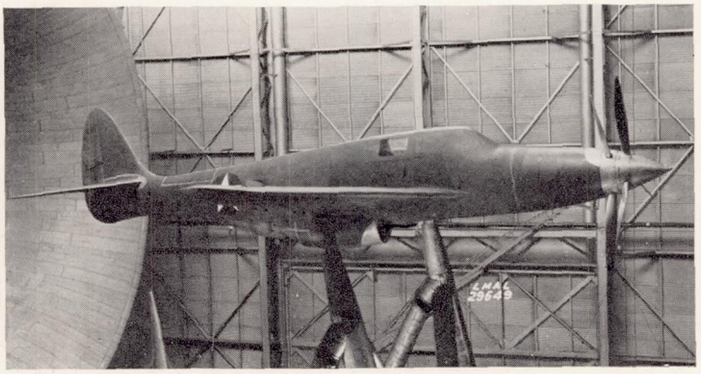

(d) Airplane 4; complete mock-up.

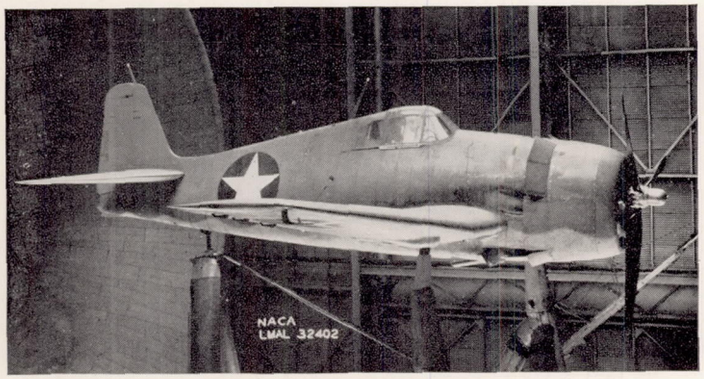

(e) Airplane 5 in service condition.

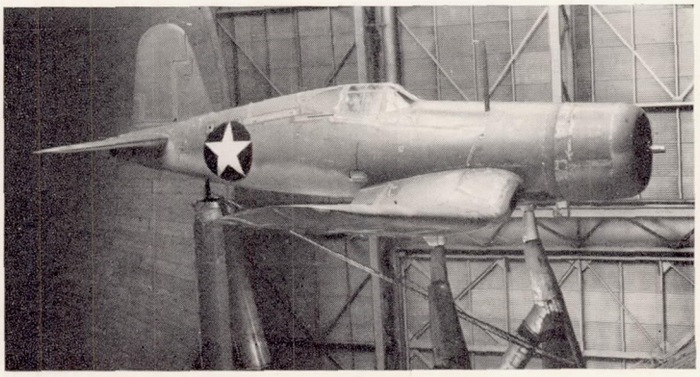

(f) Airplane 6 in service condition.

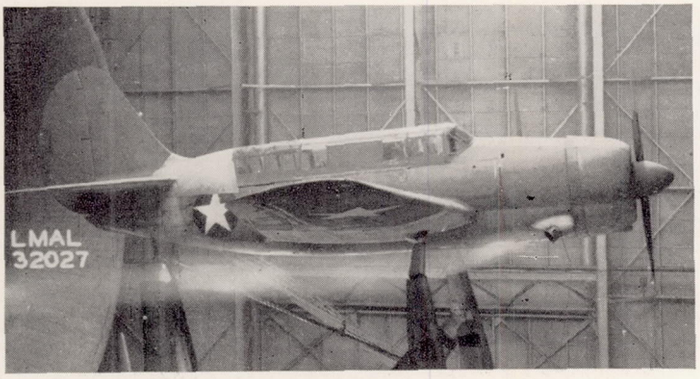

(g) Airplane 7 in service condition.

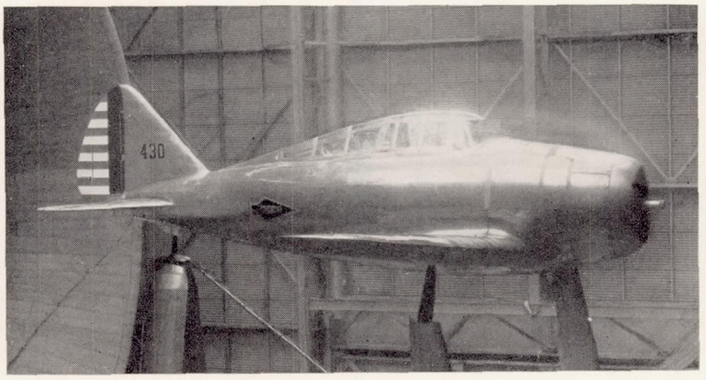

(h) Airplane 8; partially faired and sealed.

FIGURE 2.—Airplanes and mock-ups mounted for tests in Langley full-scale tunnel.

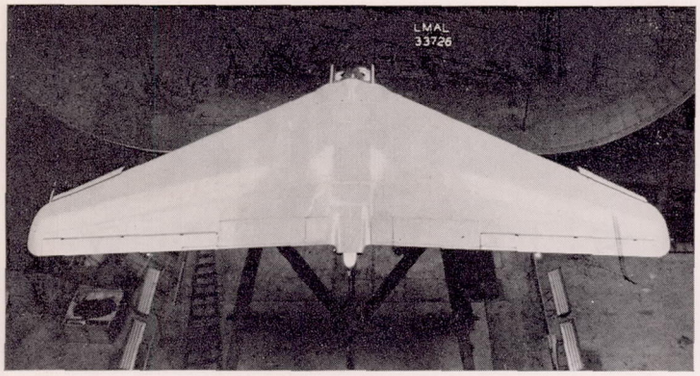

(i) Airplane 9 in service condition.

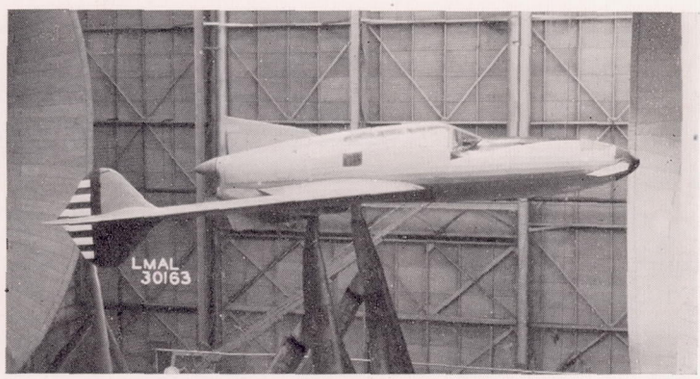

(j) Airplane 10 in service condition.

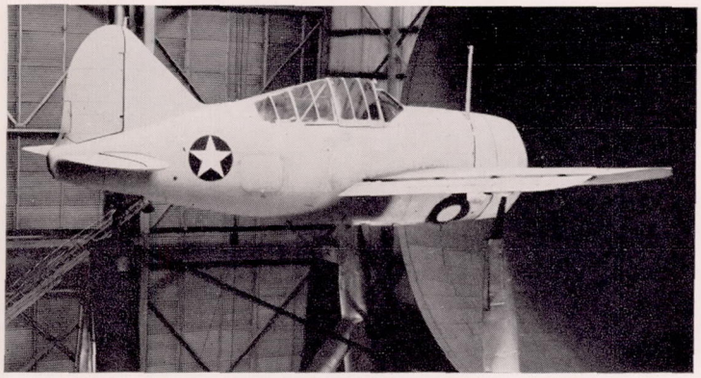

(k) Airplane 11 in service condition.

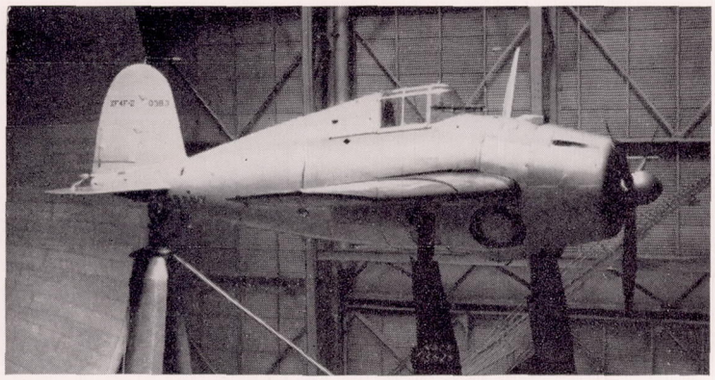

(l) Airplane 12 in service condition.

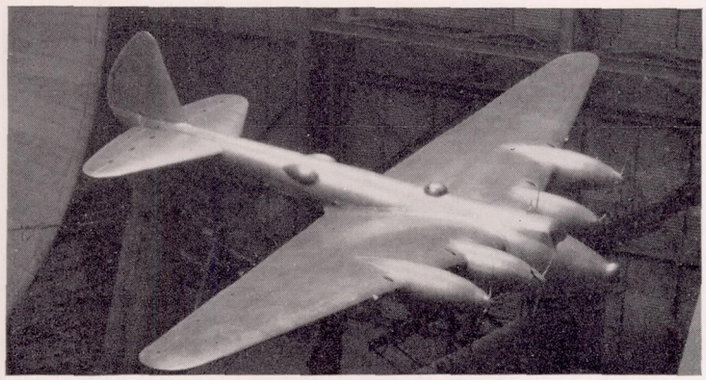

(m) Airplane 13; complete mock-up.

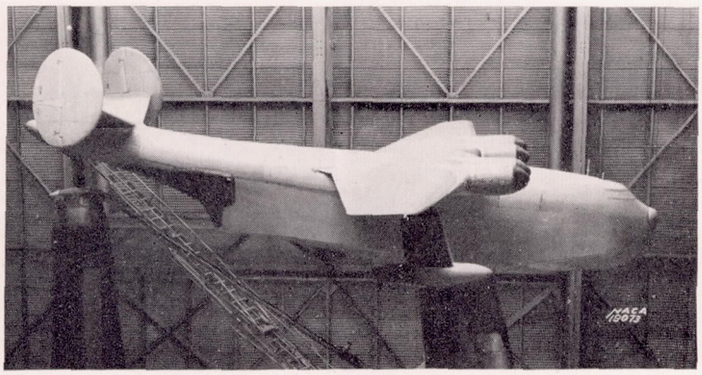

(n) Airplane 14; complete mock-up.

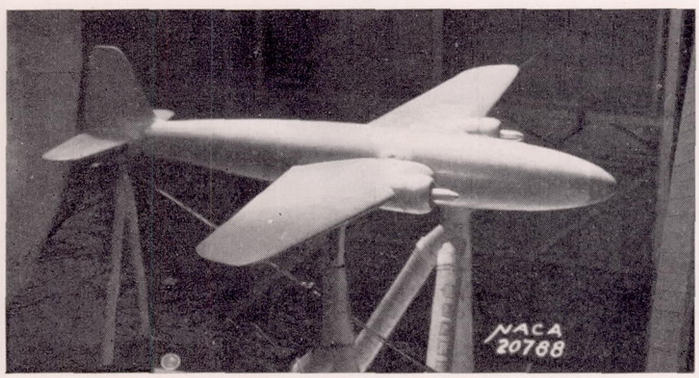

(o) Airplane 15; complete mock-up.

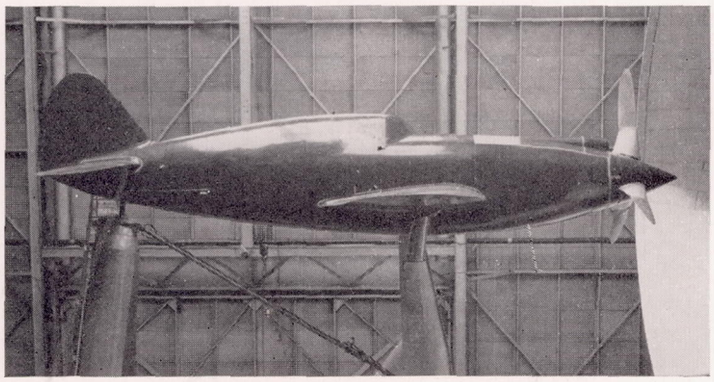

(p) Airplane 16; complete mock-up.

FIGURE 2.—Continued.

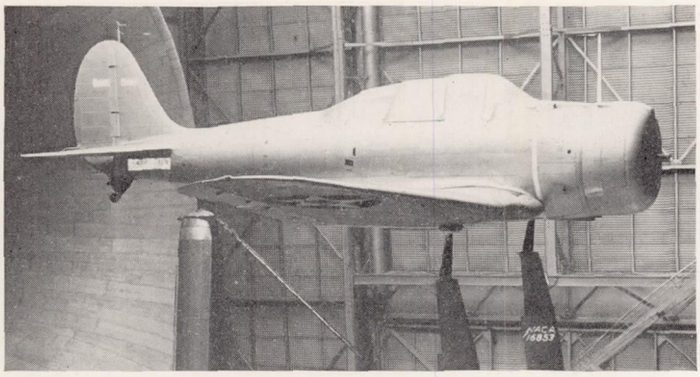

(q) Airplane 17 with revised canopy.

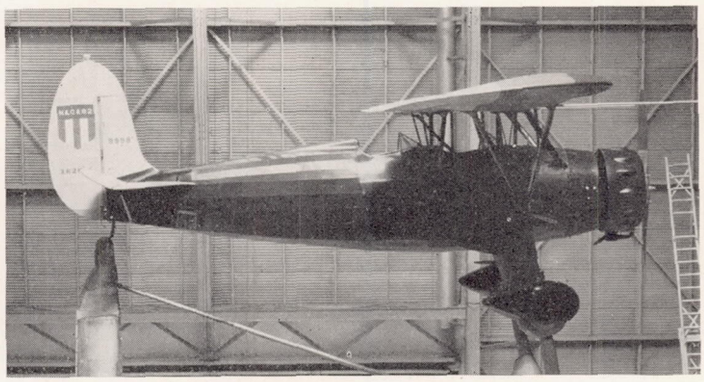

(r) Airplane 18 in service condition.

FIGURE 2.—Concluded.

TABLE I.—GEOMETRIC CHARACTERISTICS OF AIRPLANES TESTED IN LANGLEY FULL-SCALE TUNNEL

Airplane	Wing area (sq ft)	Aspect ratio	Taper ratio, $\gamma = \frac{\text{Root chord}}{\text{Tip chord}}$	Wing section [a]		Angle of incidence (deg)		Wing flaps			
				Root	Tip	Root	Tip	Type	Average flap chord / Average wing chord	Flap span / Wing span	Maximum flap deflection, $\delta_{f_{max}}$ (deg)
1	233.2	5.89	2.17	NACA–NAA compromise low drag	NACA–NAA compromise low drag	1.00	−1.25	Slotted	24.8	50.7	50.0
2	248.0	5.93	2.00	NACA 66(2x15)−116, a=0.6	NACA 66(2x15)−216, a=0.6	1.30	−.45	Plain	16.6	31.3	45.0
3	100.0	7.56	3.00	NACA 65(216)−017	NACA 67,1−(1.3)15, a=0.7	2.00	.50	do	22.1	47.0	60.0
4	284.0	5.30	1.81	NACA 66(215)−114	NACA 66(215)−213, a=0.6	1.71	−.80	Slotted	25.0	51.5	45.0
5	334.0	5.50	2.00	NACA 23016	NACA 23009	3.00	3.00	do	25.6	64.1	48.0
6	314.0	5.30	1.47	NACA 23018	NACA 23009	2.00	2.00	do	22.6	56.4	50.0
7	422.0	5.90	2.32	NACA 23017	NACA 23009	1.50	−.50	Split	23.7	61.1	60.0
8	223.7	5.90	[b]	NACA 0015	NACA 0009	1.00	1.00	do	32.0	53.3	60.0
9	250.0	5.19	4.00	NACA 66,2−018	NACA 66,2−018	0	0				
10	203.4	8.10	3.38	CW 6500−0015	CW 6500−0015	2.00	−1.50	Split	23.6	36.0	45.0
11	208.9	6.00	1.40	NACA 23018	NACA 23009	0	0	Slotted	26.6	100.0	50.6
12	233.2	5.00	1.48	NACA 23015	NACA 23009	0	0	Split	25.0	51.5	60.0
13	172.0	8.10	4.00	NACA 0018	NACA 0010	4.60	4.60	do	20.0	57.7	60.8
14	148.0	11.90	3.35	NACA 23024	NACA 23009	5.50	5.50	Slotted	[c] 28.0	[c] 53.4	55.0
15	188.0	7.70	2.50	NACA 0018	NACA 0009	2.00	2.00	Split	23.1	57.8	50.0
16	170.0	5.70	1.76	NACA 23015	NACA 23009	1.00	1.00	Slotted	25.7	55.2	40.0
17	318.6	5.40	1.96	NACA 2415	NACA 2409	2.50	2.50	Split	23.7	65.6	45.0
18	180.0	6.00	1.00	NACA $2R_112$	NACA $2R_112$	0	0				

[a] The designations of the NACA low-drag airfoils have been changed from the form furnished by the manufacturer to the form described in reference 15.
[b] Elliptical chord distribution.
[c] Only inboard and center flaps deflected.

Most of the measurements were made at tunnel airspeeds of approximately 60 miles per hour; a few tests were made at slightly lower airspeeds. In order to indicate the effect of variation in Reynolds number, measurements were made for some of the airplanes over an approximate range of tunnel velocity from 20 to 100 miles per hour.

Force readings were taken for one of the airplanes (airplane 18) at regular intervals while the angle of attack was being changed at a constant rate in order to obtain a comparison with flight measurements of maximum lift coefficient. The rate of change of angle of attack per second for these tests was varied between 0.025° and 0.200°.

The usual wind-tunnel jet-boundary and blocking corrections have been applied to all the data.

RESULTS AND DISCUSSION

The results of measurements of maximum lift coefficients and stalling characteristics of 18 airplanes tested in the Langley full-scale tunnel are summarized in the following sections. In most cases the results are given for the airplanes with landing flaps retracted and with landing flaps fully extended. The data are grouped in the first five sections to show the characteristic effects on maximum lift and stall of wing geometry, fuselages and nacelles, propeller slipstream, surface roughness and leakage, and wing leading edge appendages. In the final sections, comparisons are made of the increments of lift coefficient due to split and slotted flaps and of wind-tunnel and flight measurements of maximum lift coefficients of airplanes.

WING GEOMETRY

Conventional plan forms.—Stall progressions for airplanes with untwisted wings of different taper ratios (airplanes 13, 12, and 8) are presented in figure 3 for landing flaps retracted and fully deflected. Although these data are given for complete airplanes with fuselages and nacelles but with propellers removed, the results show trends generally characteristic of the effects of wing taper ratio on the progression of the stall.

With the landing flaps retracted (fig. 3(a)), local areas of separation appeared on airplane 13 (wing taper ratio, 4:1) at the wing trailing edge near the fuselage and behind oil-cooler outlets located just outboard of each nacelle for relatively low angles of attack; the main stall, however, started at the wing tips and progressed inboard with increasing angle of attack. Theoretical studies (references 2 to 4) show that, for plain untwisted wings of high taper ratio, the section

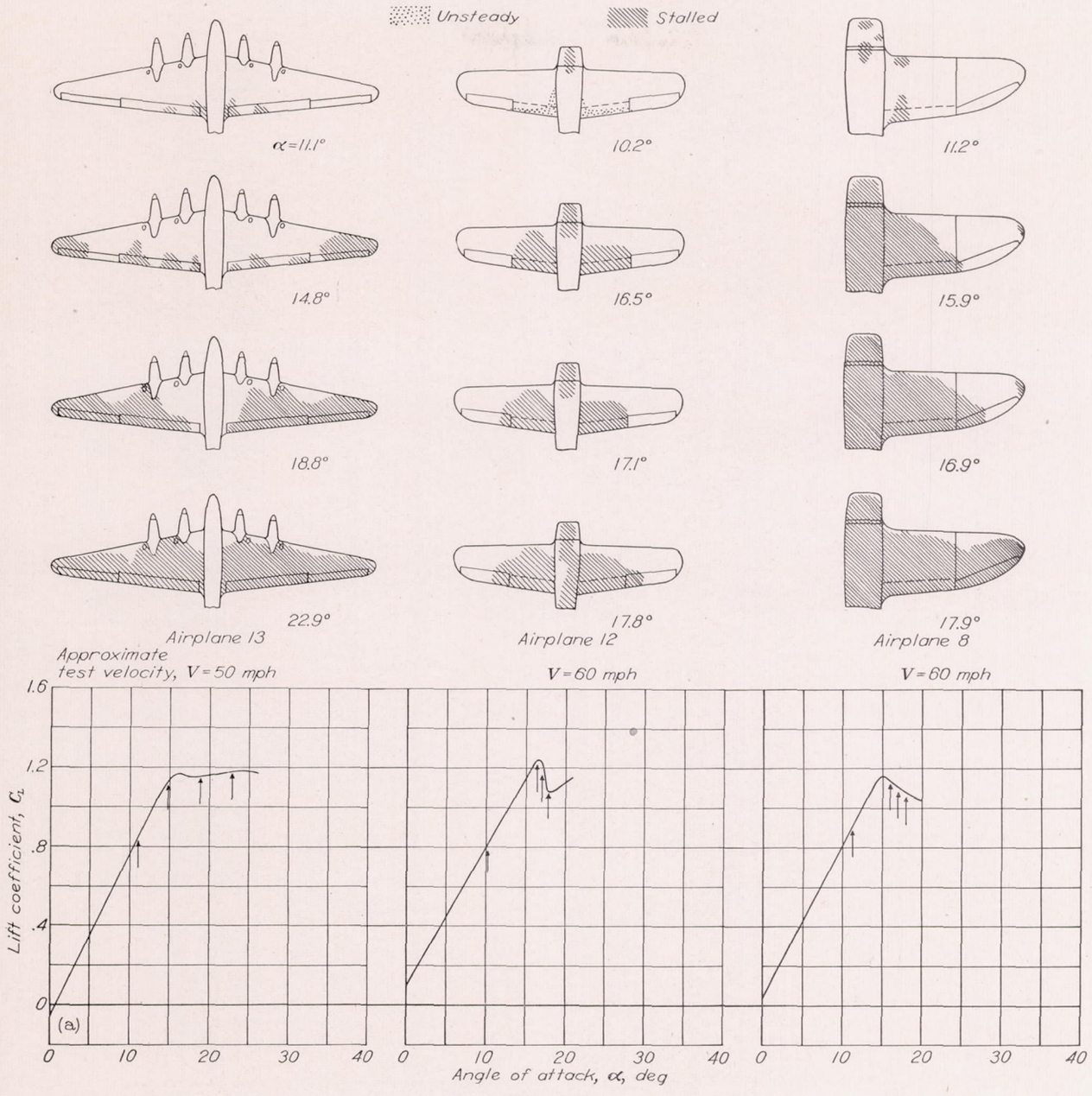

(a) Flaps retracted.

FIGURE 3.—Stall progressions for airplanes with wings of different taper ratios. Complete airplanes less propellers.

lift coefficients are highest near the wing tip and these sections should therefore be the first to approach maximum lift. Tip stall is further precipitated on highly tapered wings by the spanwise variation of section Reynolds number (reference 4). For airplane 13, the Reynolds number of the tip sections is thus about one-fourth that of the root sections and the tip sections tend to stall first.

Owing to the loss in aileron effectiveness and damping in roll usually associated with wing-tip stall, several methods have been devised for moving the location of the initial stall inboard. These methods, which include washout, central sharp leading edges, leading-edge tip slats, and increases in camber from root to tip, are discussed in detail in reference 4. A backward movement of the maximum camber of the wing sections from root to tip will also generally improve the stall (reference 5).

Stalling characteristics for an airplane with a wing of low taper ratio (airplane 12), for which $\lambda=1.48$, are shown in figure 3(a). For this airplane, stall initially occurred at the wing root and progressed outboard with increasing angle of attack but did not include the wing tips for the range of angle of attack tested. Unlike highly tapered wings, the section lift coefficients are highest at the root for wings with low taper ratio. High section lift coefficients at the root, together with the interference effect of the fuselage, should cause the stall to occur initially at the root sections for airplanes with wings of low taper ratio. The Reynolds number effect previously discussed for the highly tapered wing is relatively unimportant for wings of low taper ratio.

Airplane 8, which has a wing with elliptical chord distribution, exhibited stall ng characteristics somewhere between those for an airplane with a wing of high taper ratio and

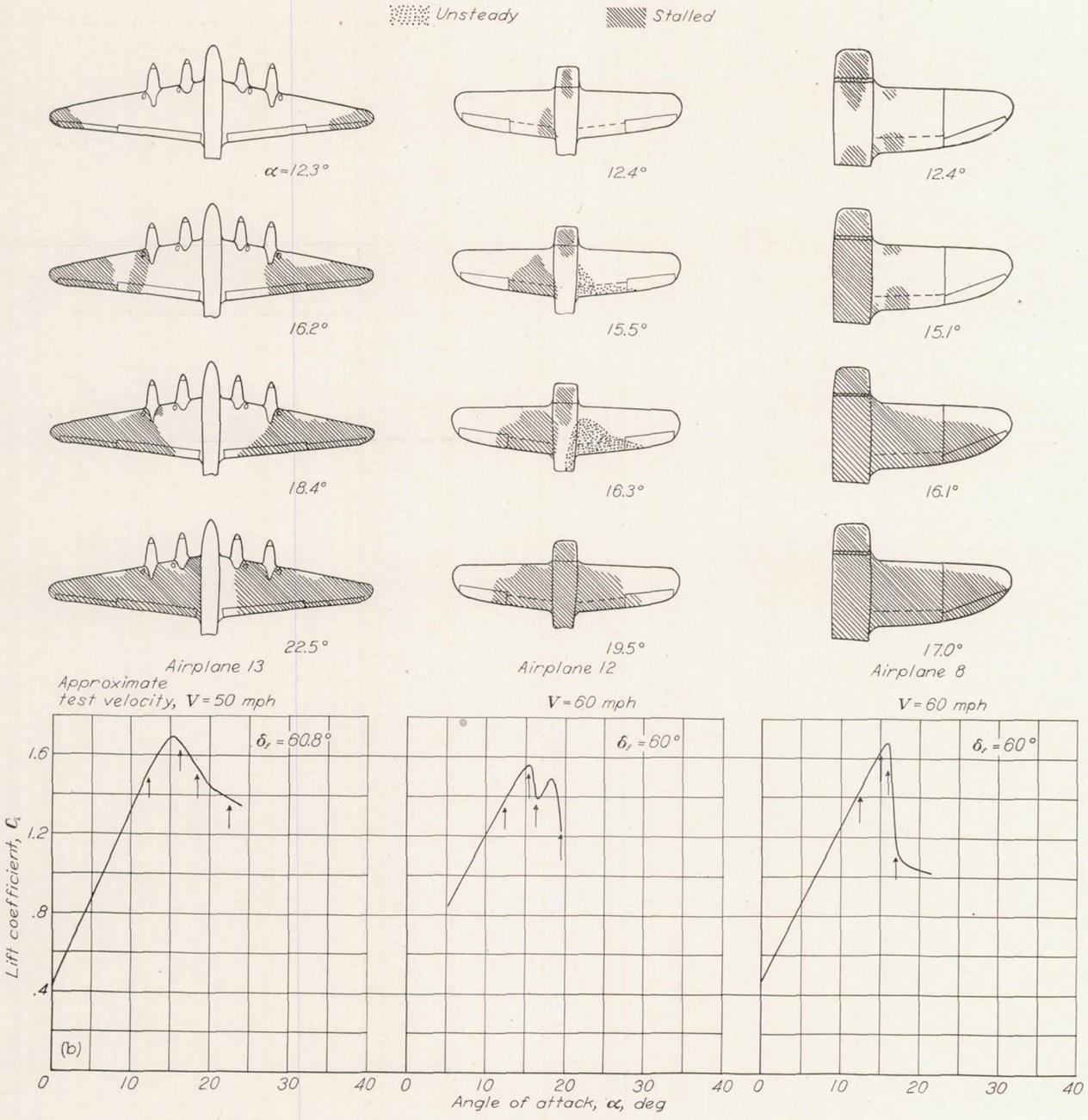

(b) Maximum flap deflection.

FIGURE 3.—Concluded.

those for an airplane with a wing of low taper ratio. Stall initially occurred at the root section but, as the angle of attack was increased, the wing tips began to stall. Further increases in angle of attack caused the two regions of stall to merge at about one-third of the semispan inboard from the wing tips.

Extending the landing flaps to maximum deflection for airplanes 13, 12, and 8 produced the stall progressions shown in figure 3(b). For all three airplanes, flap deflection generally tended to "clean up" the inboard sections of the wing. No small areas of separation appeared at the wing trailing edge near the root section of airplane 13 and the stall progressions for airplanes 12 and 8 showed that, at similar angles of attack below the angle of maximum lift, smaller portions of the wings of these three airplanes were stalled with flaps deflected than with flaps retracted.

A particularly undesirable condition near the maximum lift coefficient was exhibited by airplane 8 with the landing flaps deflected. A rapid increase in the area of separation with a change of only 1° in angle of attack was observed and the lift decreased rapidly with small increases in angle of attack above the angle of maximum lift (fig. 3(b)). Flight observations of the stalling characteristics of this airplane with flaps extended showed a strong tendency for the airplane to ground-loop to the left in the three-point attitude. A brief study of this condition in flight, with the aid of tufts attached to the wing surfaces, indicated that an asymmetrical stalling of the wing occurred at the time the ground-looping tendency developed.

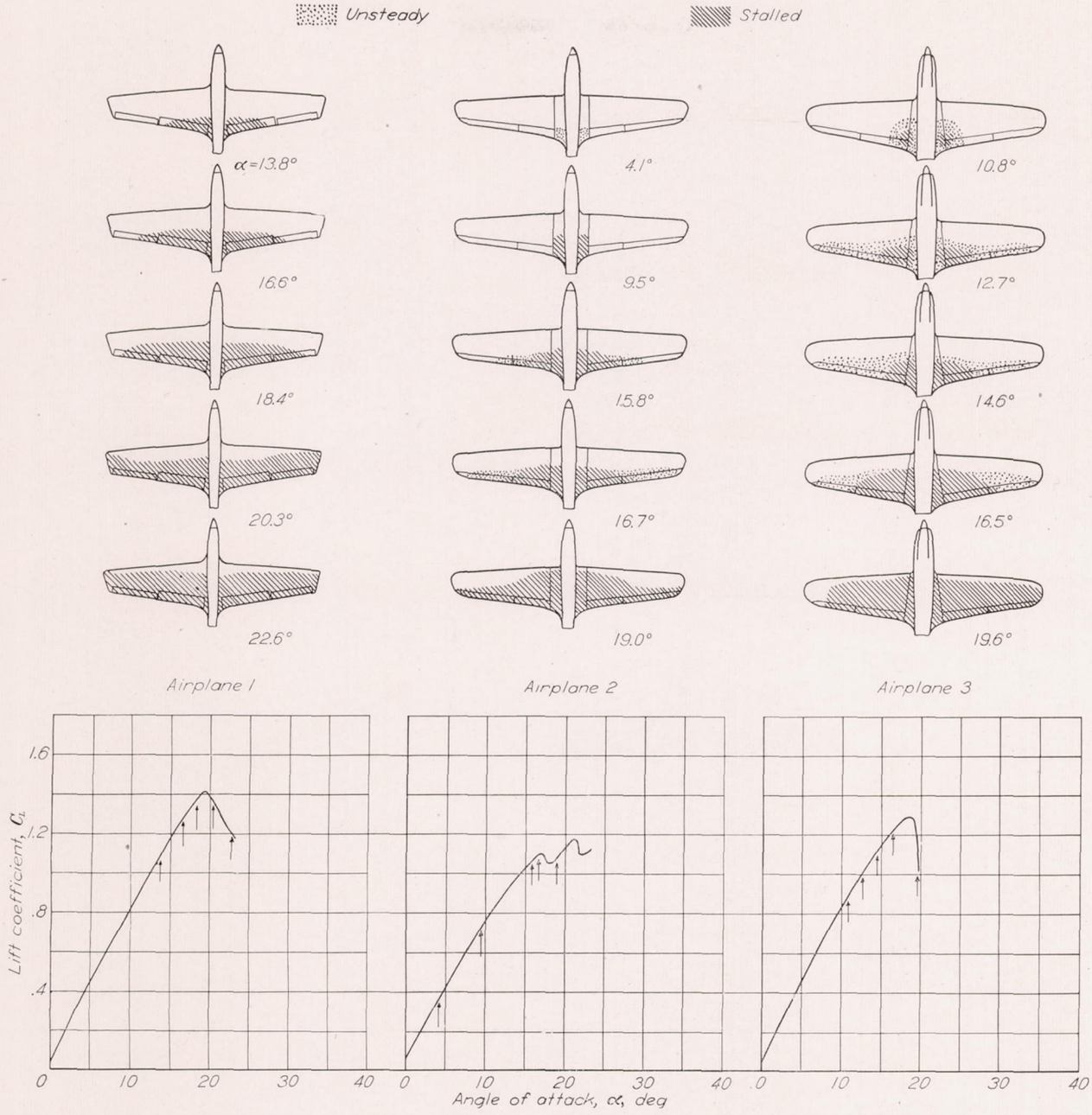

FIGURE 4.—Stall progressions for three present-day airplanes having low-drag wings. Complete airplanes less propellers; $\delta_f=0°$; approximate test velocity, 60 miles per hour.

The exact nature of the effects of flap deflection on the stalling characteristics of airplanes is not well defined. Flight observations of a large number of airplanes tested in the United States and in England (references 5 and 6) have indicated that flap deflection either improved or aggravated the stall in about an equal number of cases. Flap deflection generally tends to aggravate the stall by increasing the upwash over the outer unflapped parts of the wing and by cleaning up the area of separation at the root. On the other hand, the handling characteristics of an airplane in flight near the stall may be improved by flap deflection if the flap wake envelops the tail at angles of attack near the stall and thus produces a stall warning either by tail buffeting or by a rapid change in trim due to the loss in tail effectiveness.

Stall progressions for three typical present-day pursuit airplanes having twisted wings of low-drag airfoil sections (airplanes 1, 2, and 3) are shown in figure 4. The taper ratio and washout of the wings of these three airplanes are nearly the same. (See table I for wing details.) The stalls are strikingly similar; separation begins, in each case, at the wing-fuselage juncture and progresses outboard along the rearward portion of the wing with increasing angle of attack. The stalling characteristics of these airplanes, as interpreted from the tuft observations, are probably good. Although airplane 3 shows a rapid loss in lift after the stall, no serious trouble should be encountered by the pilot inasmuch as the root-section stall should provide adequate warning of the approach of $C_{L_{max}}$.

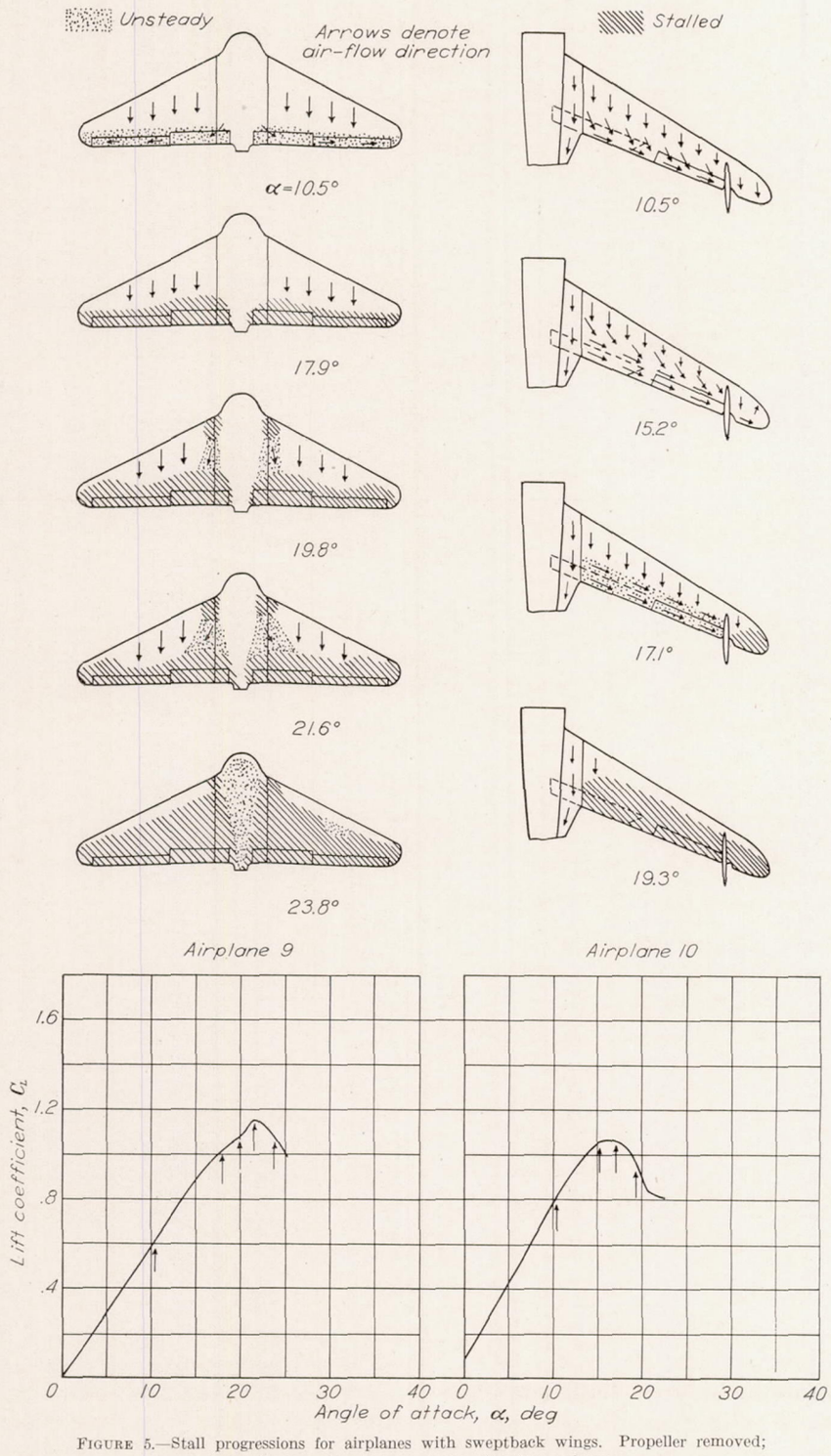

FIGURE 5.—Stall progressions for airplanes with sweptback wings. Propeller removed; $\delta_f=0°$; approximate test velocity, 60 miles per hour.

Sweptback wings.—The effect of sweepback on the stalling behavior is illustrated in figure 5 by tuft observations for airplanes 9 and 10. According to the tuft observations, these airplanes should have poor stalling characteristics. The control surfaces of airplane 9 are stalled at an angle of attack well below that for $C_{L_{max}}$. For airplane 10, the initial stall occurred at the wing tips and the area of separation spread rapidly inboard along the wing trailing edge with increasing angle of attack. In both cases, the air flow over the upper wing surfaces near the trailing edge, prior to stalling, was toward the wing tips.

The spanwise location of the initial stall on a sweptback wing is primarily dependent on the spanwise flow of the boundary layer on the suction surface (reference 7). On a sweptback wing, the surface pressure gradients sweep the slower moving air of the boundary layer toward the tip. The thicker boundary layer near the tip tends to stall the wing first in that region. Inasmuch as the trailing edge of the wing of airplane 10 has a greater amount of sweepback than that of airplane 9, the surface pressure gradients between

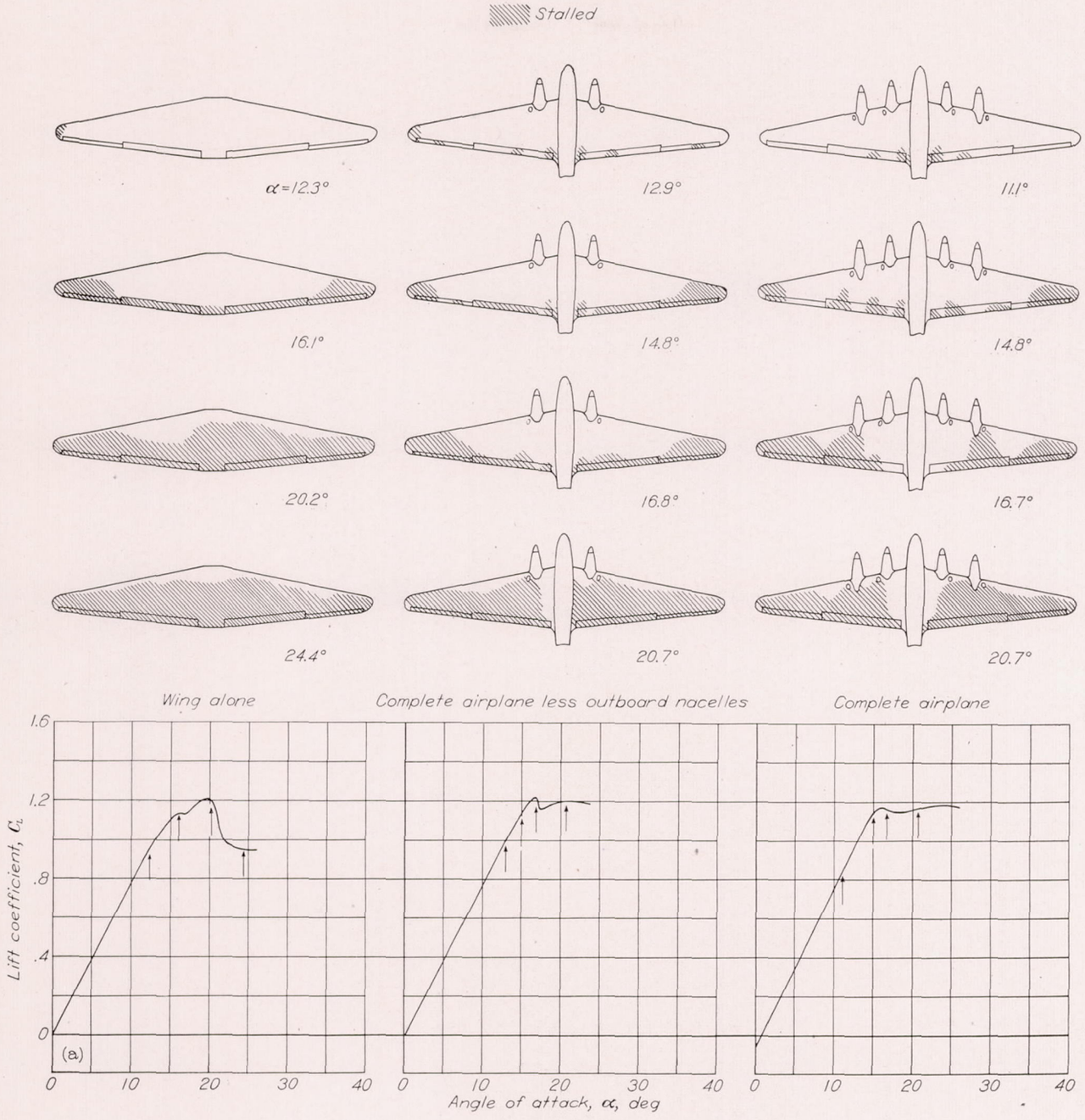

(a) Flaps retracted.

FIGURE 6.—Effect of fuselage and nacelles on the stalling characteristics of airplane 13. Propellers removed; approximate test velocity, 50 miles per hour.

chordwise sections near the trailing edge of the wing of airplane 10 are stronger than the pressure gradients on airplane 9. The flow toward the wing tip and the wing tip stall should therefore be more pronounced on airplane 10 than on airplane 9 and figure 5 shows that such is the case.

FUSELAGES AND NACELLES

The addition of a fuselage and nacelles to a wing frequently introduces centers of local separation that may reduce the maximum lift of the airplane but will usually improve the handling characteristics of the airplane near the stall. When the flow separates from the inner sections of the wing, the downwash at the tail is reduced and a nose-down pitching moment results, which tends to decrease the areas of separation. Furthermore, the wakes from the wing-fuselage juncture and the nacelles may cause a stall warning by reducing the effectiveness of the tail or by producing tail buffeting.

The effects of fuselages and nacelles on the maximum lift and stalling characteristics of two models of four-engine airplanes (airplanes 13 and 14) are shown in figures 6 and 7. Figure 6 shows lift curves and stall progressions for airplane 13 with the landing flaps retracted and deflected 60.8° for the wing alone, for the airplane with outboard nacelles off, and for the complete airplane. With the landing flaps retracted (fig. 6(a)), the stall progression for the wing alone was characteristic of a highly tapered untwisted wing. The addition of the fuselage and two inboard nacelles caused

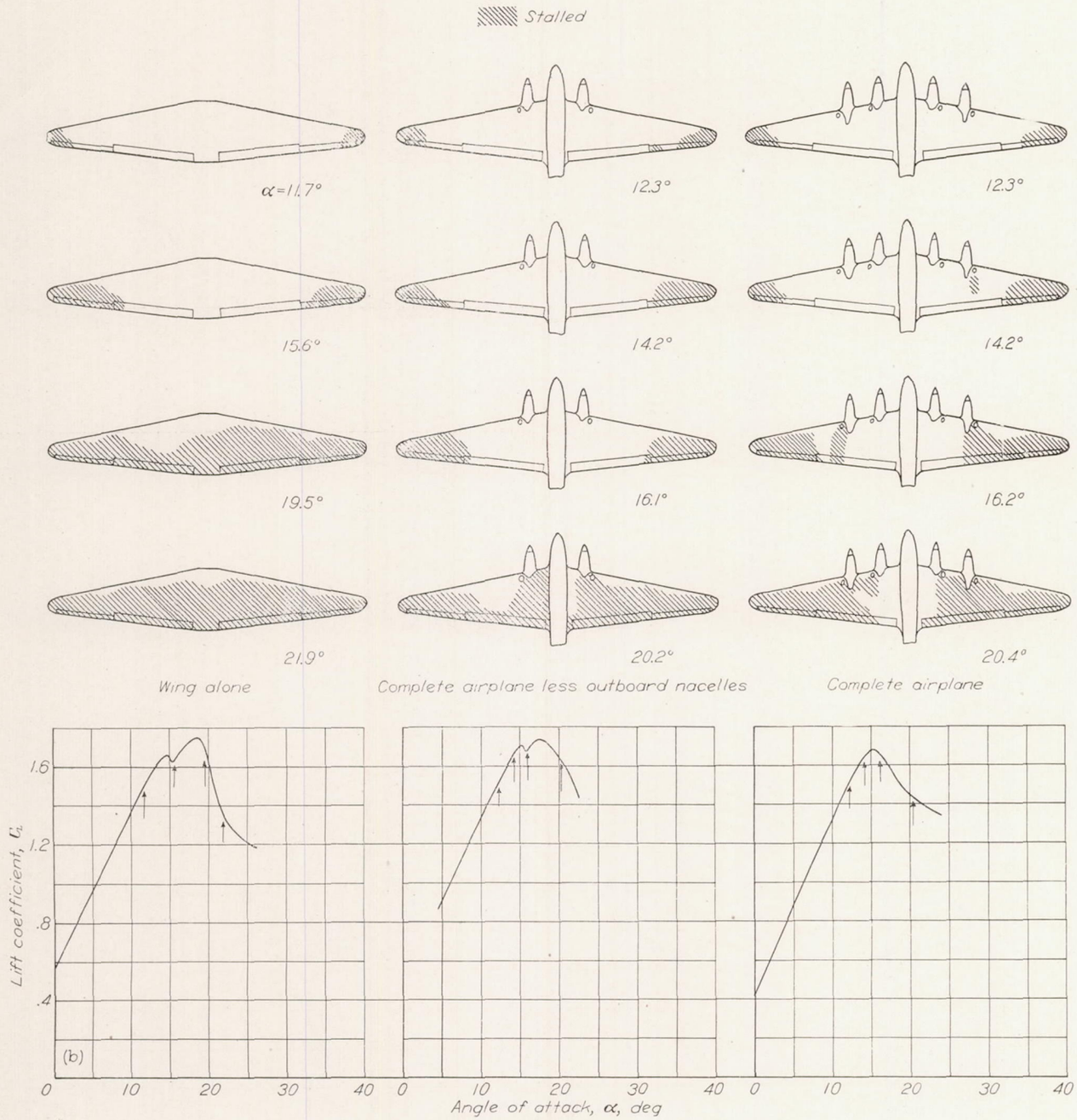

(b) Flaps deflected 60.8°.

FIGURE 6.—Concluded.

local areas of separation to appear at the trailing edge of the wing adjacent to the fuselage and behind the nacelles and oil-cooler outlets prior to the main stall, which started at the wing tips. When the outboard nacelles were added to the model, additional stalled areas, which were particularly noticeable behind the oil-cooler outlets, appeared at the lower angles of attack. Flap deflection (fig. 6(b)) generally cleaned up the inboard sections of the wing. As for the case with the flaps retracted, the addition of the outboard nacelles with the landing flaps deflected 60.8° reduced the $C_{L_{max}}$ of the airplane and caused premature areas of separation behind the oil-cooler outlets near the outboard nacelles. Tuft observations of airplane 13 in flight (unpublished) showed stall patterns very similar to those observed in the wind tunnel. The power-off stalls, as observed by the pilot, were characterized by a relatively slow roll-off and small angles of roll. Adequate stall warning was given by a decrease in the effectiveness of the elevators and rudder and by a relatively large change in the required control movement. The stall patterns were practically the same with the landing flaps up or down and with the landing gear up or down.

Stall progressions and lift curves for a model of a large flying boat (airplane 14) are shown in figures 7(a) and 7(b) for landing flaps retracted and deflected 55°, respectively. For the wing alone with flaps retracted, stall initially occurred at the center section. The area of separation spread outboard along the flaps with increasing angle of attack and

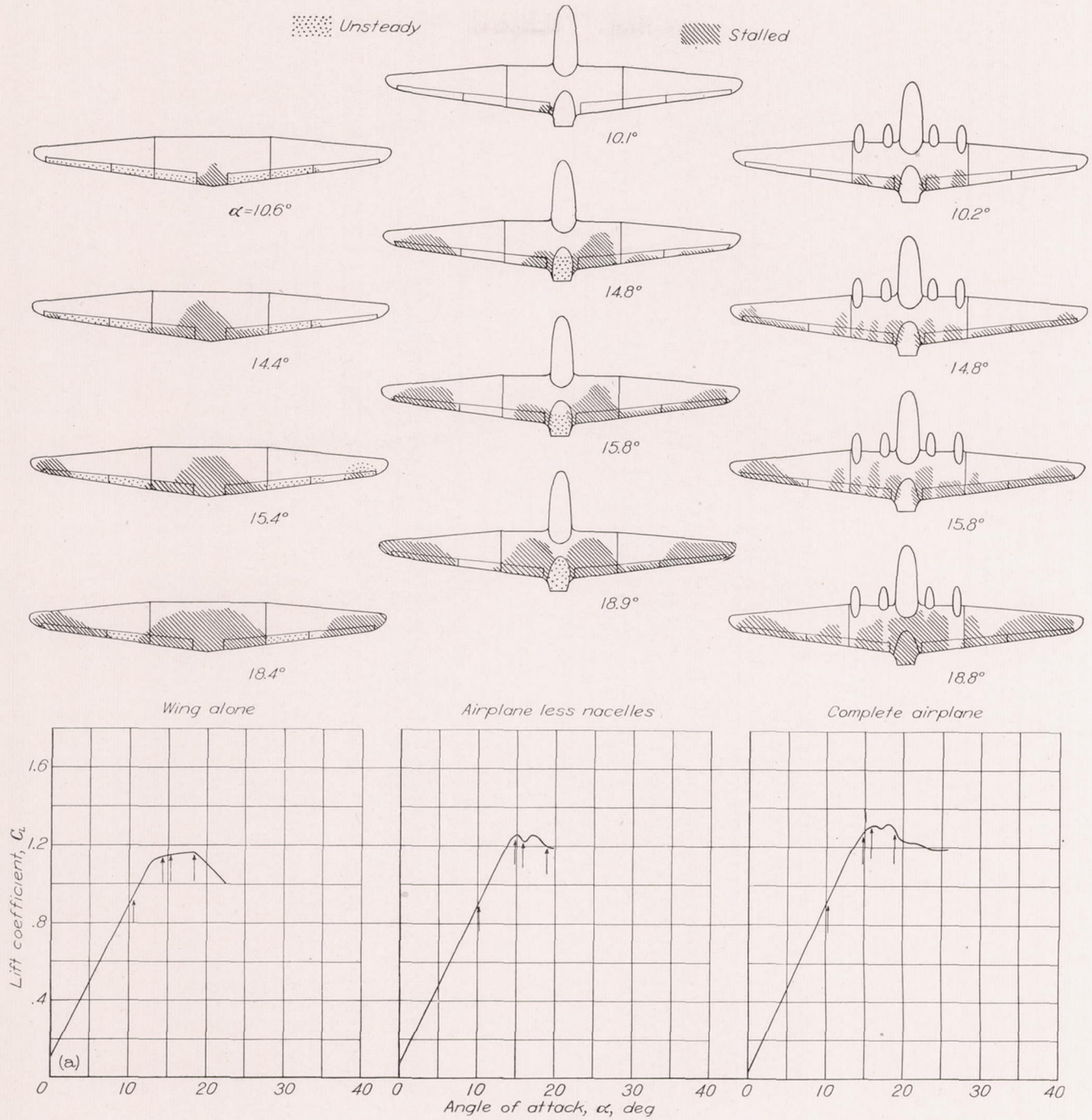

(a) Flaps retracted.

FIGURE 7.—Effect of fuselage and nacelles on the stalling characteristics of airplane 14. Propellers removed; approximate test velocity, 60 miles per hour.

merged with the tip stall, which started after the maximum lift coefficient had been reached. Although this wing would be expected to stall first at the tips because of its high taper ratio ($\lambda=3.35$), root stall occurred first, probably because the thick NACA 23024 airfoil section at the root has a lower maximum section lift coefficient than the NACA 23009 section at the tip at the test Reynolds number. Addition of the fuselage to the wing delayed the stall about 2° and increased the maximum lift coefficient about 0.10. With four nacelles added to the wing, local areas of separation occurred directly behind the nacelles at relatively low angles of attack. The maximum lift coefficient of the model with the nacelles on, however, was about 0.06 higher than with the nacelles removed and is attributed to the increased effective wing area due to the nacelles.

Deflecting the landing flaps 55° for the wing-alone condition (fig. 7(b)) resulted in essentially the same stall patterns as observed with the flaps retracted, except that the stalled areas over the unflapped portions of the wing were slightly larger for corresponding angles of attack owing to the induced upwash over those sections. For the complete airplane, deflecting the flaps 55° removed the local areas of separation behind the nacelles that were observed with the flaps retracted and also increased the area of separation near the wing tips. No data were available for the airplane with nacelles removed and flaps deflected.

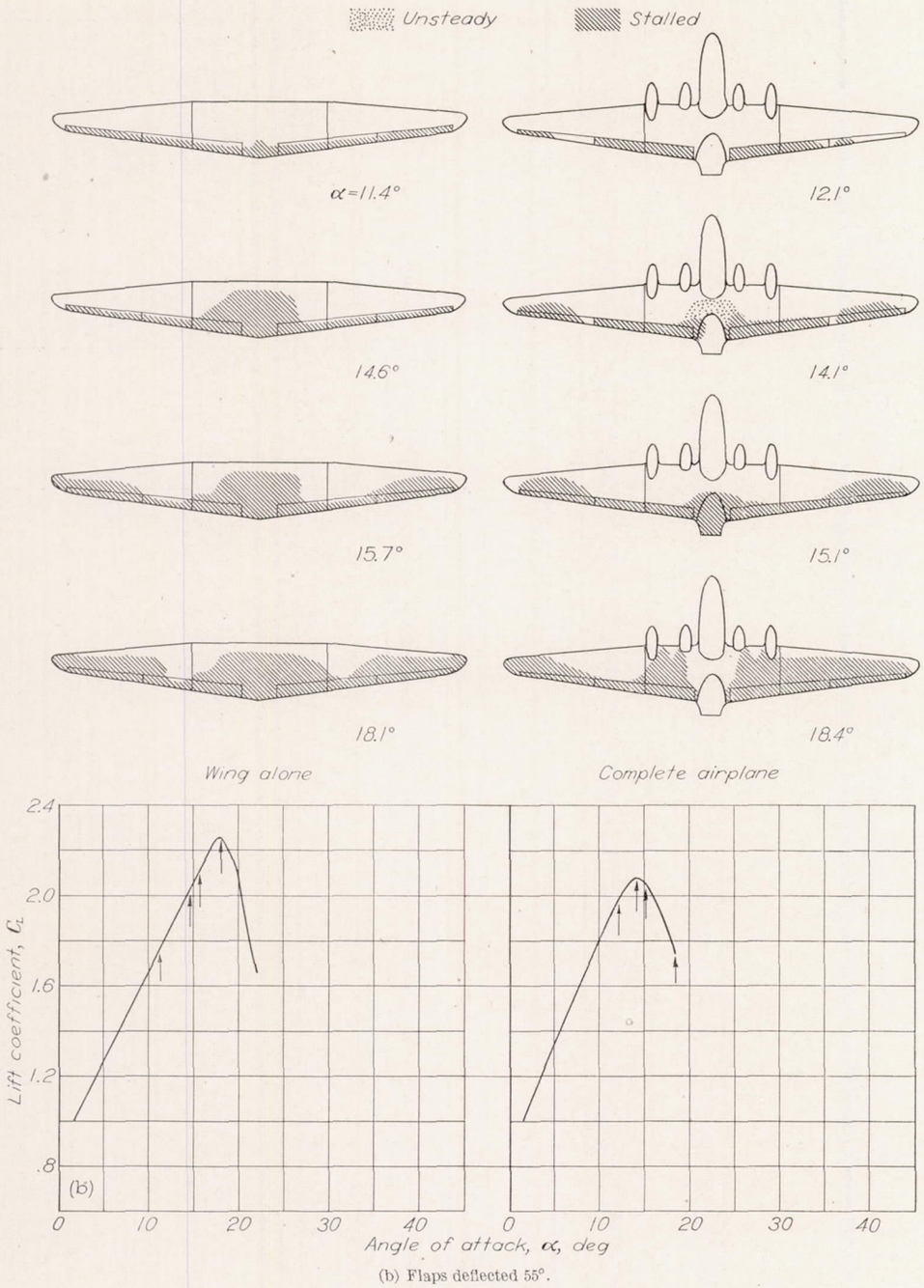

(b) Flaps deflected 55°.

FIGURE 7.—Concluded.

PROPELLER SLIPSTREAM

The large changes in the stalling characteristics of airplanes that result from propeller operation are usually attributed to the separate effects of the increased axial velocity within the slipstream and of the slipstream rotation. The increased velocity within the slipstream tends to clean up the inboard sections of the wings by increasing the local Reynolds number and thus delaying separation along the sections directly behind the propeller. The rotation within the slipstream increases the effective angle of attack of the wing section behind the upgoing propeller blades and decreases the effective angle of attack of the wing section behind the downgoing propeller blades. An asymmetrical stall pattern is thus produced. In addition to these effects, the downwash behind an inclined propeller tends to reduce the effective angles of attack of the sections behind the propeller and thereby delays the occurrence of stall.

The effects of propeller operation on the stalling characteristics of airplane 6 are shown in figure 8. With the propeller removed, the stall progression with angle of attack was fairly similar for both wings; with the propeller operating at a thrust coefficient T_c of 0, however, the wing section behind the upgoing propeller blades stalled at a considerably lower angle of attack than the wing section behind the downgoing propeller blades. Increasing T_c to 0.2 decreased the asymmetry of the stall that was measured at $T_c=0$, owing to the fact that the increased slipstream velocity had a greater effect than the increased slipstream rotation.

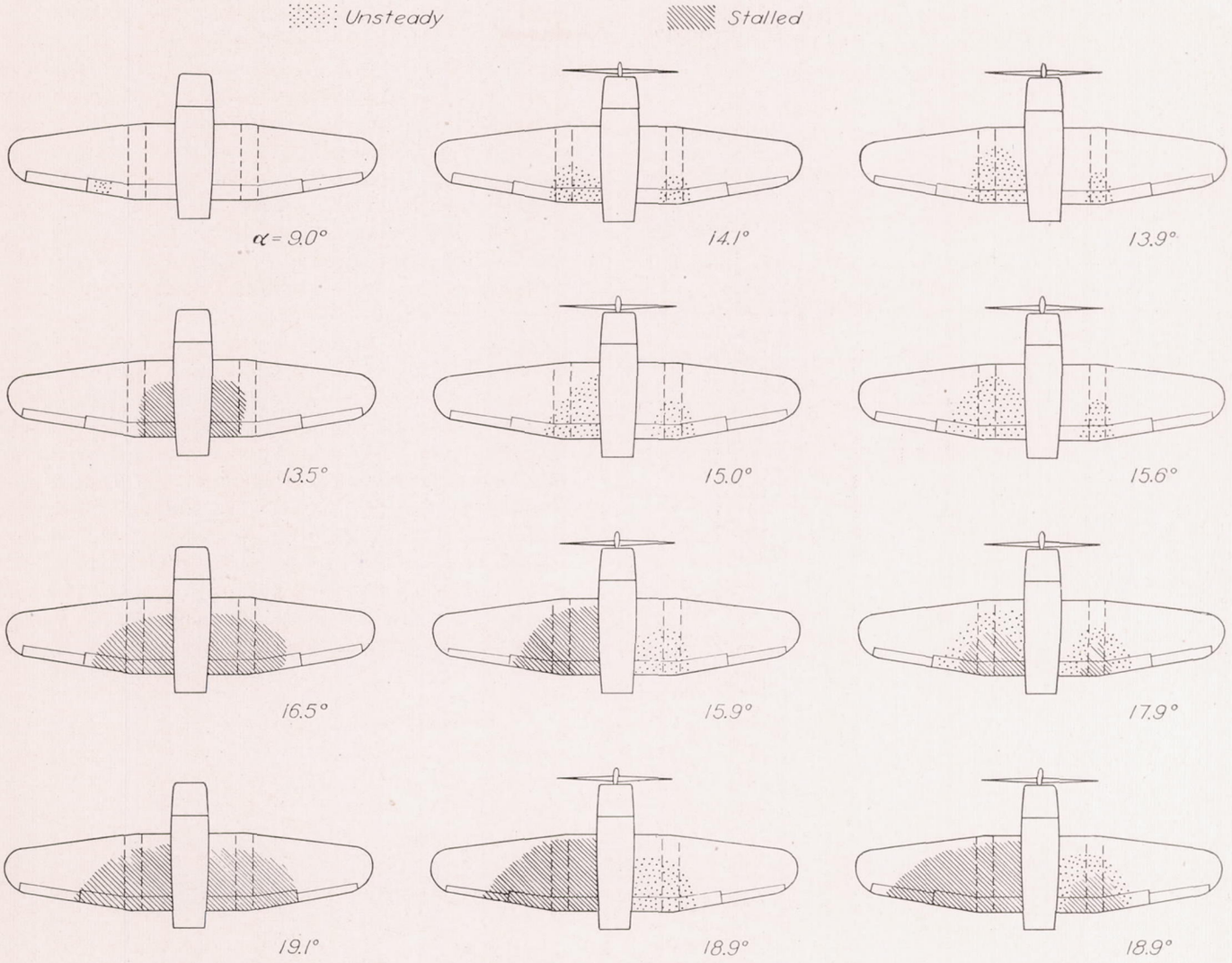

FIGURE 8.—Effect of propeller slipstream on the stalling characteristics of airplane 6. Airplane in service condition; $\delta_f = 50°$; approximate test velocity, 60 miles per hour.

Flight measurements of the stalling characteristics showed that airplane 6 developed a serious left-wing dropping tendency during power-on landings. In order to check these results, measurements were made of the variation of rolling-moment coefficient with angle of attack of the airplane with the propeller removed and operating. The results of these measurements are given in figure 9. With the propeller removed, the rolling-moment coefficient of the airplane was essentially independent of angle of attack; with the propeller operating at $T_c=0.2$, however, the rolling-moment coefficient changed slowly from -0.008 at $\alpha=8°$ to -0.024 at $\alpha=17.0°$ (angle of maximum lift). Above $\alpha=17.0°$ a sharp increase in rolling-moment coefficient, which would be sufficient to cause serious rolling instability during power-on landings, occurred.

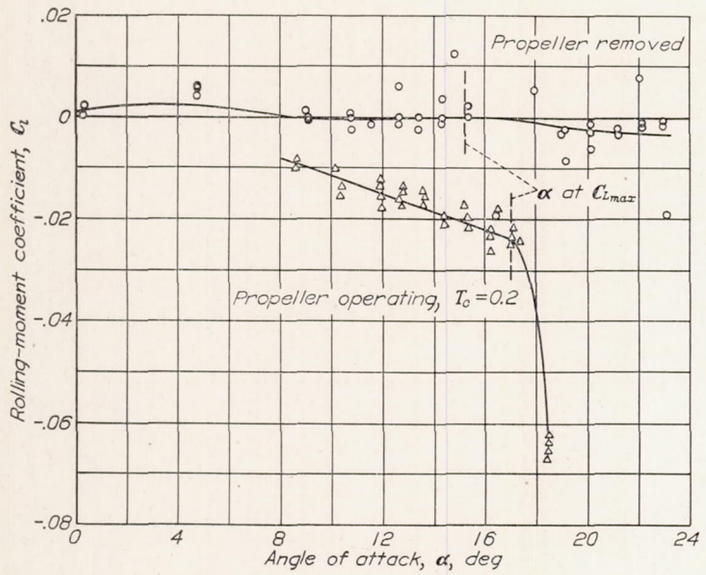

FIGURE 9.—Effect of propeller operation on the rolling moments of airplane 6. Airplane in service condition; $\delta_f=50°$; approximate test velocity, 60 miles per hour.

In an attempt to improve the power-on stalling characteristics of airplane 6, a sharp leading edge was installed on the right wing as shown in figure 10. The results of tuft observations and lift and rolling-moment measurements made with the sharp leading edge installed on the wing are also shown in figure 10. In general, the sharp leading edge should considerably improve the stalling characteristics of the airplane, inasmuch as the asymmetry of the stall pattern at high angles of attack was decreased and the large variation of rolling-moment coefficient with angle of attack was eliminated. The maximum lift coefficient of the airplane, however, was reduced from 2.30 to 1.88 by the sharp leading edge.

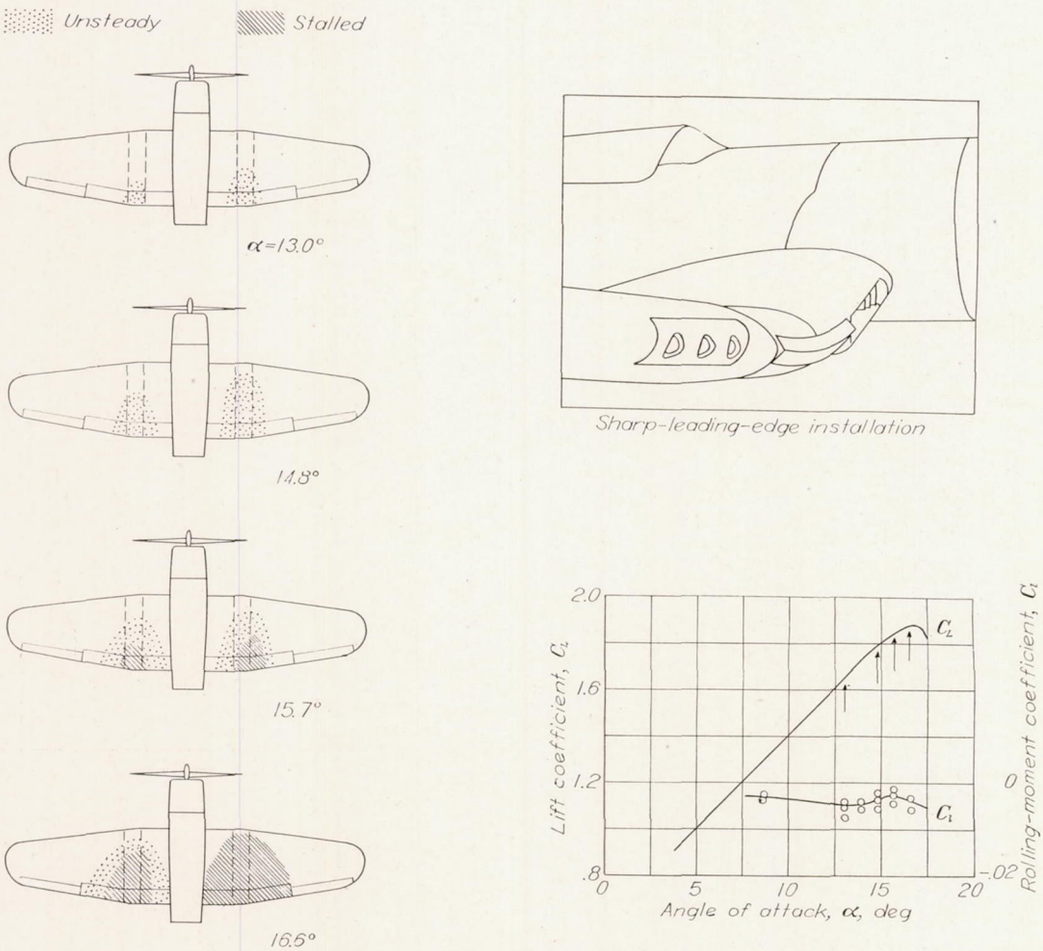

FIGURE 10.—Effect on the stalling characteristics and rolling moments of installing a sharp leading edge on the right wing of airplane 6. Propeller operating; $T_c=0.2$; $\delta_f=50°$; approximate test velocity, 60 miles per hour.

The effects of the propeller slipstream on the maximum-lift and stalling characteristics of airplane 16 with the flaps retracted are shown in figure 11. With the propeller idling, little difference in the progression of the stall on the right and left wings was noted. At $T_c=0.013$, however, a greater percentage of the wing was stalled on the side of the upgoing propeller blades than on the side of the downgoing propeller blades for equal angles of attack. The maximum lift coefficient was about 0.05 higher with the propeller operating at $T_c=0.013$ than with the propeller idling.

Stall progressions for two four-engine monoplane models (airplanes 13 and 14) with propellers operating are shown in figures 12 and 13. The effects of the propeller slipstream on the stalling characteristics of airplane 13 may be obtained by comparing figures 6 and 12. Propeller operation ($T_c\approx0.30$) cleaned up the areas of separation behind the nacelles so that the outboard wing sections were stalled at $C_{L_{max}}$ whereas the inboard wing sections were unstalled. This condition may result in handling difficulties near the stall owing to a probable loss in aileron effectiveness and damping in roll. Flight tests of airplane 13 with power on and flaps retracted, however, resulted in stalls characterized by a relatively slow roll-off and small angle of roll. The development of the rolling instability was gradual and the roll could be stopped immediately by a reduction in angle of attack. These stalling characteristics, as measured in flight, can probably be explained by reference to figure 12 which shows that, for all angles of attack, the stalled areas on the right and left wing surfaces are very nearly equal; the development of any rolling motion would therefore be gradual.

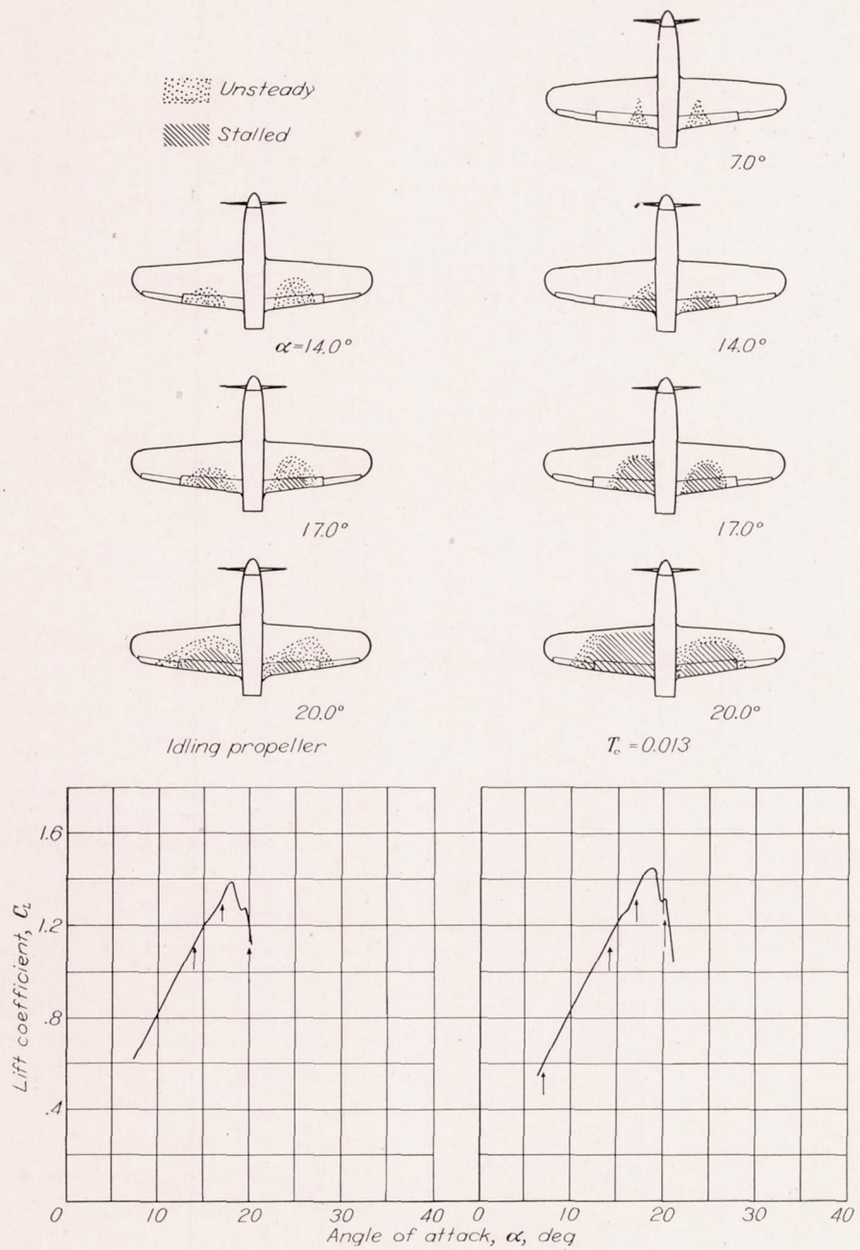

FIGURE 11.—Effect of propeller slipstream on the stalling characteristics of airplane 16.
$\delta_f=0°$; approximate test velocity, 60 miles per hour.

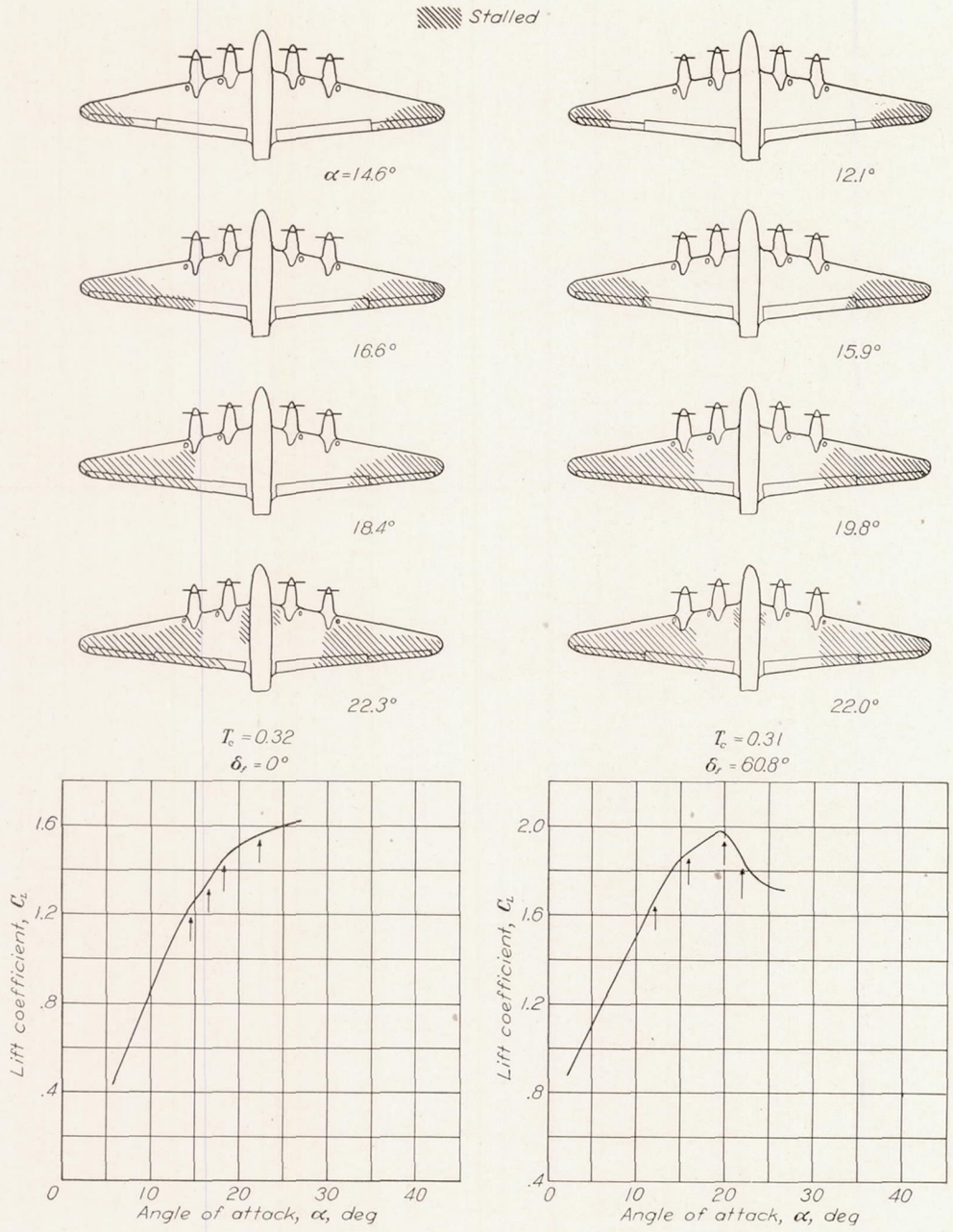

FIGURE 12.—Effect of propeller slipstream on the stalling characteristics of airplane 13. Approximate test velocity, 50 miles per hour.

The effects of the propeller slipstream on the maximum lift and stalling characteristics of airplane 14 with landing flaps retracted and deflected 55° are shown in figure 13. Comparison of figure 13 with figure 7, which gives stall progressions for airplane 14 with the propeller removed, indicates that in this case the stall progressions were not altered appreciably at the low values of T_c (T_c=0.03 with flaps retracted and T_c=0.09 with flaps deflected), although the maximum lift coefficients were increased from 1.32 to 1.38 with flaps retracted and from 2.08 to 2.17 with flaps deflected. Increasing the thrust coefficients to 0.13 with flaps retracted and to 0.15 with flaps deflected decreased the percentage of the wing area behind the propeller that was stalled at the lower thrust coefficients and further increased the maximum lift coefficients to 1.53 with flaps retracted and to 2.28 with flaps deflected.

WING SURFACE ROUGHNESS AND LEAKAGE

Because of increased armament requirements, wings of present-day military airplanes must be equipped with numerous access doors, inspection plates, gun ports, ammunition-ejection slots, and many other items that tend to make the wings extremely rough and to allow air leakage through the wings. In several cases it has been found that the $C_{L_{max}}$ may be increased appreciably by relatively simple modifications of the wings. In order to show the extent to which wing roughness and air leakage affect the maximum lift coefficient of an airplane, data are presented in figures 14 to 16 for three present-day military airplanes (airplanes 6, 5, and 1). The data include lift measurements with the wings in the service condition and with the wings faired and sealed in attempts to increase the maximum lift coefficients of these airplanes.

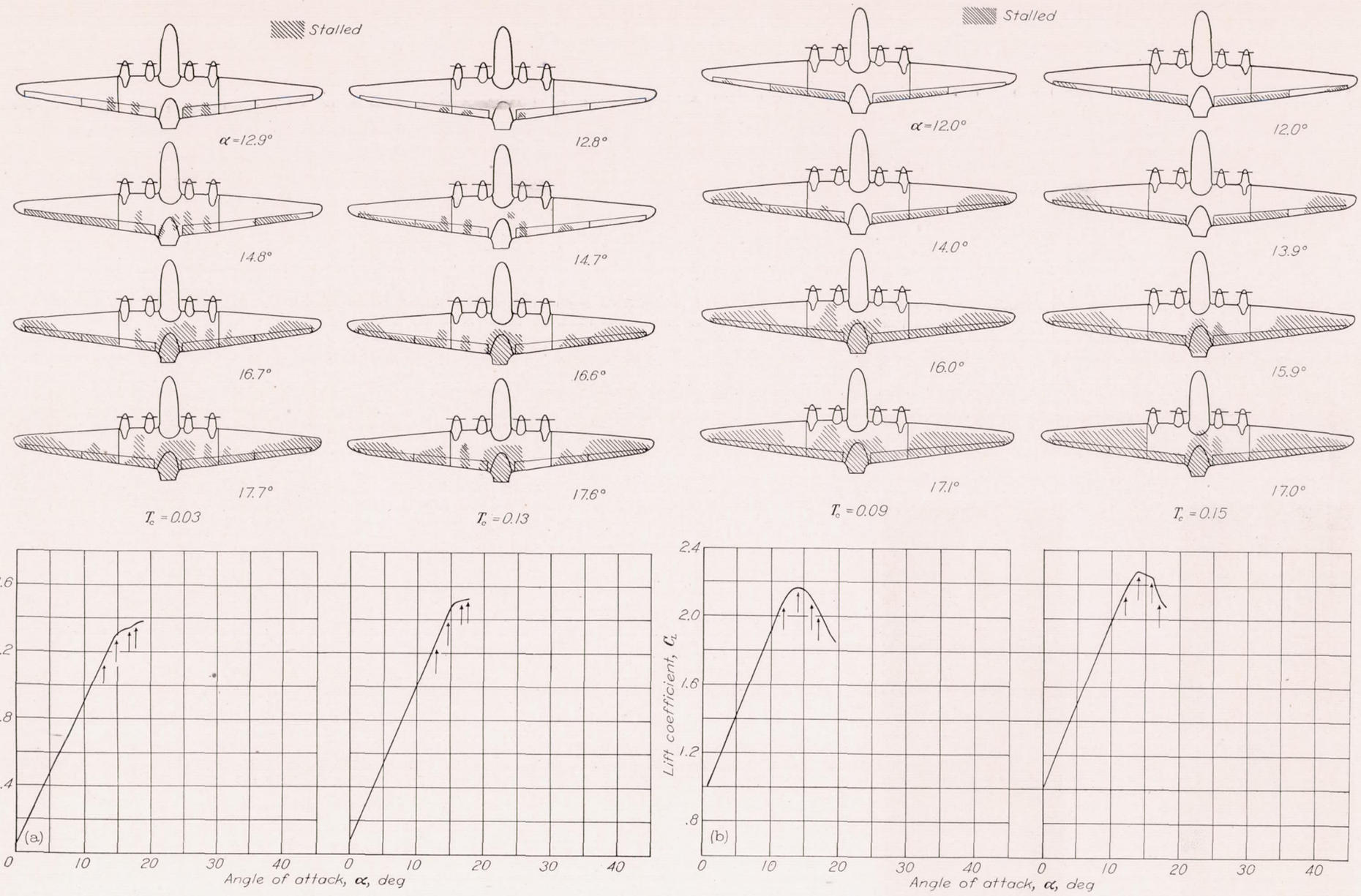

(a) Flaps retracted. (b) Flaps deflected 55°.

FIGURE 13.—Effect of propeller slipstream on the stalling characteristics of airplane 14. Approximate test velocity, 60 miles per hour.

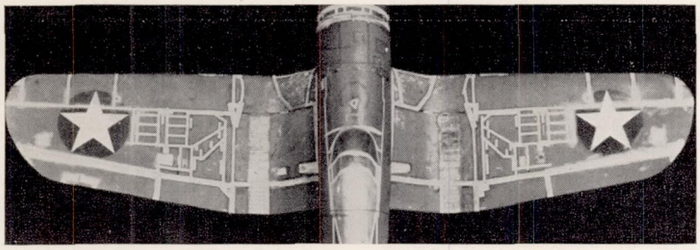

Wing faired and sealed

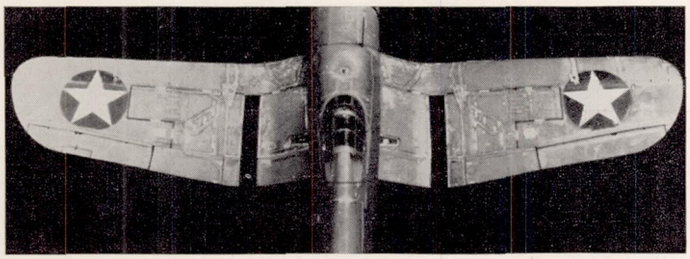

Service wing

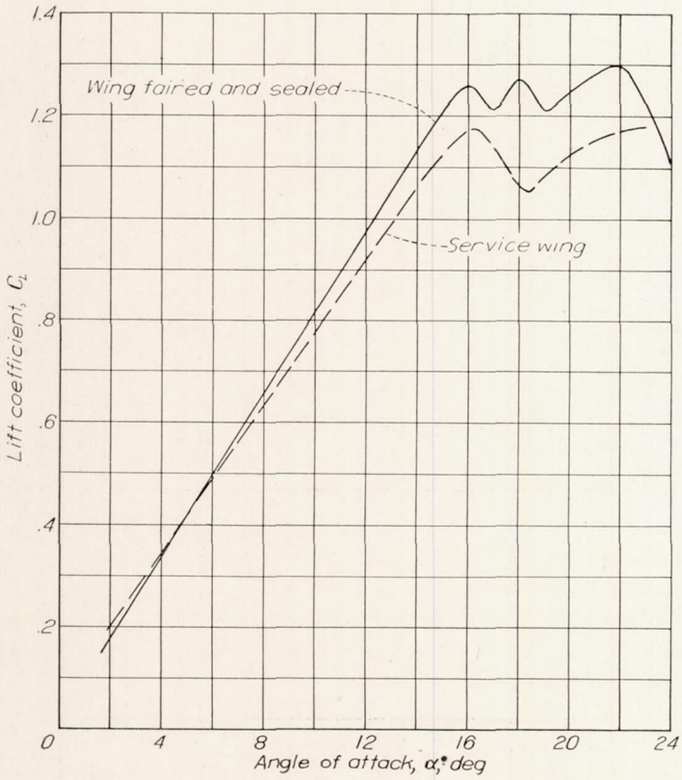

FIGURE 14.—Effect of wing surface roughness on the $C_{L_{max}}$ of airplane 6. Propeller removed; $\delta_f = 0°$; approximate test velocity, 60 miles per hour.

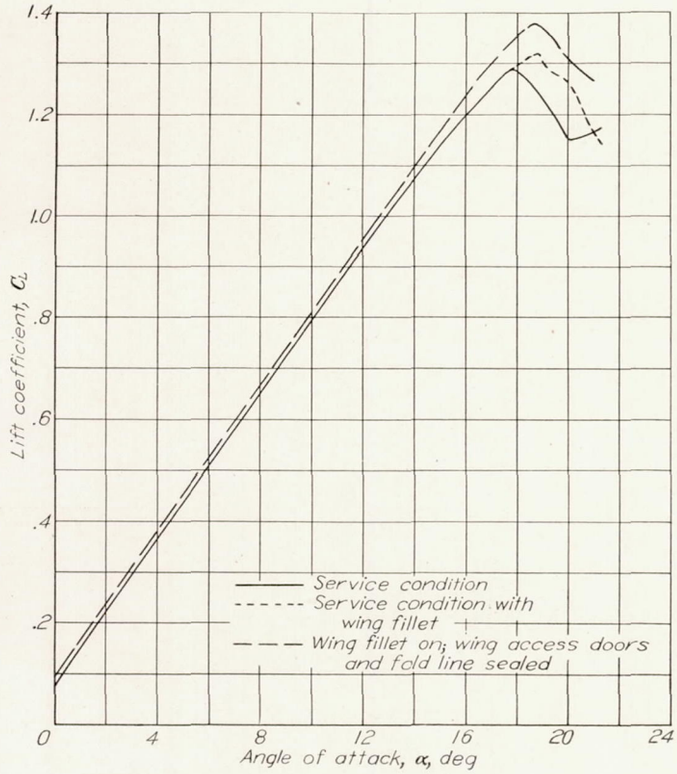

FIGURE 15.—Effect of wing surface roughness on the $C_{L_{max}}$ of airplane 5. Propeller removed; $\delta_f = 0°$; approximate test velocity, 60 miles per hour.

The maximum lift coefficients obtained for airplane 6 with the wing in service condition and with the wing completely faired and sealed are compared in figure 14. As shown by the photographs included in figure 14, the service wing has an exceptionally large number of cover plates, access doors, and construction irregularities. In addition, a rough walkway projects more than ⅛ inch from the wing surface and the wing fold line leaves a large gap in the wing. The maximum lift coefficient was only 1.17 for this airplane with the wing in the service condition. When the wing was faired and sealed by masking tape, as shown in figure 14, the $C_{L_{max}}$ was increased to 1.26. The tape seals eliminated leakage through the wing; nevertheless, the wing was not smooth and the $C_{L_{max}}$ remained relatively low.

The effects of surface roughness on the maximum lift coefficient of airplane 5 are shown in figure 15. A fillet was installed at the wing-fuselage juncture of this airplane to eliminate the sharp break along the juncture, but the increase in $C_{L_{max}}$ was only 0.03. Sealing the wing access doors and the fold line further increased the $C_{L_{max}}$ by 0.06. It is noted that the variation of airfoil section from the root to the tip of the wing of this airplane is nearly similar to that of airplane 6; the maximum lift coefficients obtained for airplane 5 in the service condition and with the wing faired and sealed, however, are about 0.10 higher than the corresponding

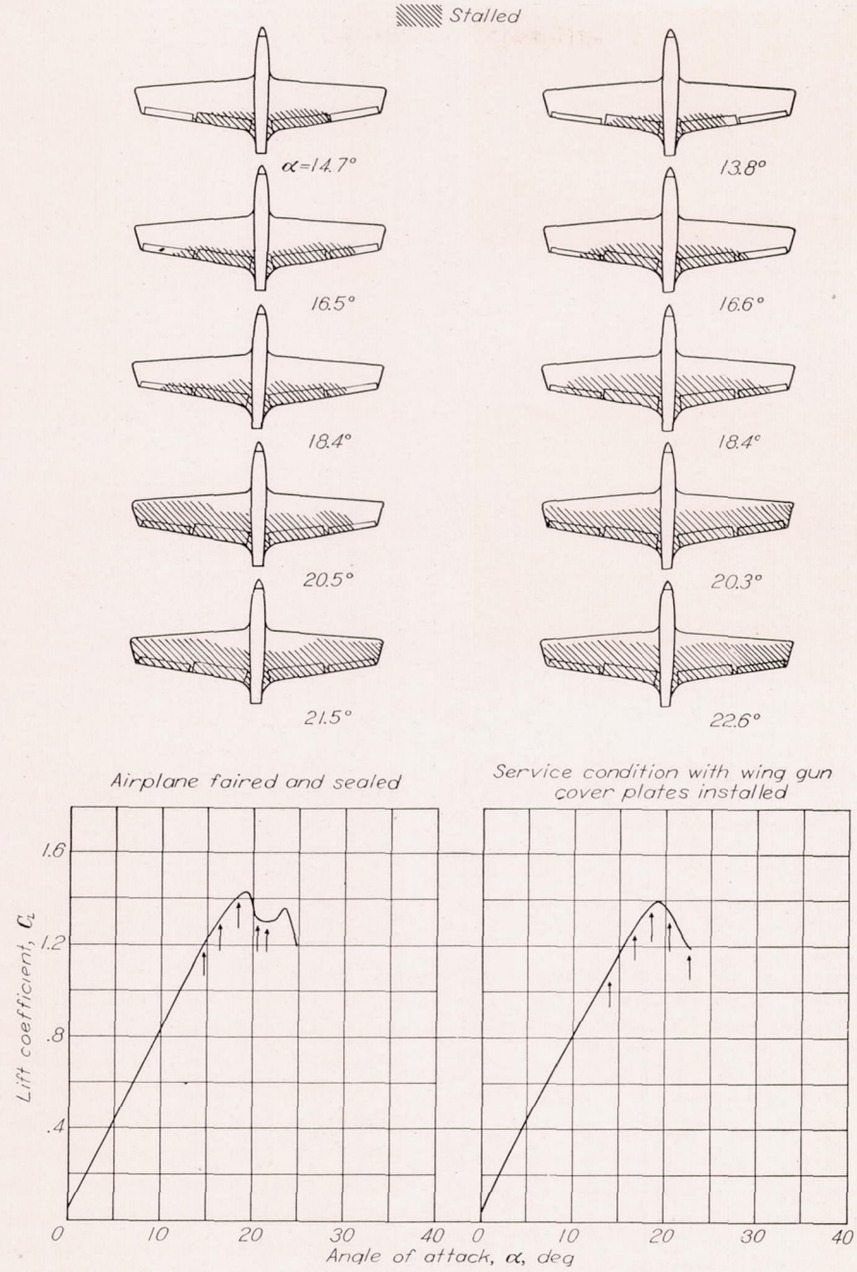

FIGURE 16.—Effect of wing surface roughness on the stalling characteristics of airplane 1. Propeller removed; $\delta_f=0°$; approximate test velocity, 60 miles per hour.

coefficients for airplane 6. This difference is attributed chiefly to the fact that the wing of airplane 5 was aerodynamically "cleaner" than the wing of airplane 6.

Stall progressions, in addition to lift-coefficient data, are given in figure 16 to show the effects of surface roughness on airplane 1, which has a low-drag wing. The wing of this airplane is exceptionally clean aerodynamically inasmuch as the few access doors and cover plates are set smoothly into the wing with no apparent breaks in the wing contour. The maximum lift coefficient of 1.44 for the faired and sealed condition and of 1.40 for the service wing are higher than those obtained for airplanes 5 and 6. The stall patterns show that the stalled areas of the faired and sealed wing were always slightly less, at corresponding angles of attack, than the stalled areas of the service wing.

WING LEADING-EDGE APPENDAGES

Armament.—Some of the results of an investigation to determine the effects on maximum lift coefficient of various machine-gun and cannon installations on the wing of

Test conditions						$C_{L_{max}}$ flaps down	α at $C_{L_{max}}$ (deg)
Gun position	Wing	Gun stations	Barrel extensions	Breech fairing	Mounting post fairing		
Basic condition—smooth airplane						2.00	16.8
Low	Right	2, 3, 4	Flush	On	On	1.98	17.3
Low	Right	1, 2, 3, 4	Flush	On	On	1.94	16.3
Low	Right	1, 2, 3, 4	Flush	On	Off	1.99	17.3
Low	Right	1, 2, 3, 4	10 in	On	On	1.91	16.3
High	Left	1, 2, 3, 4	Flush	On	On	1.99	17.2
High	Left	1, 2, 3, 4	2 in	Off	On	1.86	15.5
Low	Right	1, 2, 3, 4	10 in	Off	Off	1.87	16.4
Low	Right	1, 2, 3, 4	18 in	Off	Off	1.91	16.6
High [1]	Left	1, 2, 3, 4	Flush	On	On	1.96	17.4

[1] Modified gun sleeves.

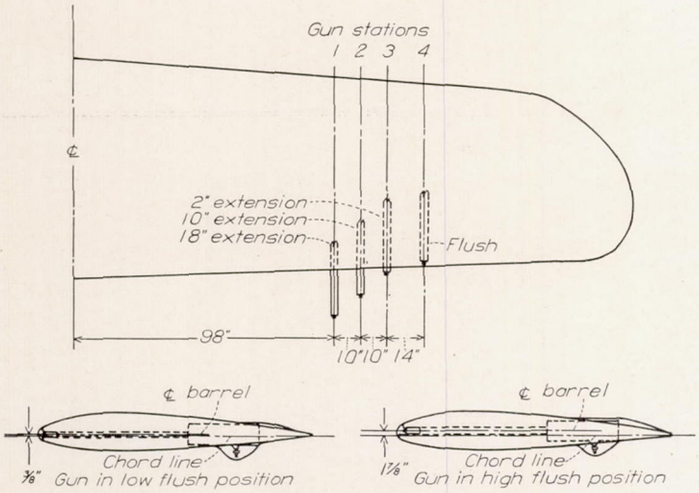

FIGURE 17.—Effect of various machine-gun (0.50-caliber) installations on the maximum lift coefficient of airplane 11.

Test conditions	Wing	Cannon fairing	Magazine fairing	$C_{L_{max}}$ flaps down	α at $C_{L_{max}}$ (deg)
Underslung installation 1, $h=9\frac{1}{4}$ in.	Right and left	On	On	1.91	17.3
Underslung installation 2, $h=6\frac{3}{4}$ in.	Right and left	On	On	1.95	16.8
Completely submerged installation	Right and left	On	On	1.96	17.0

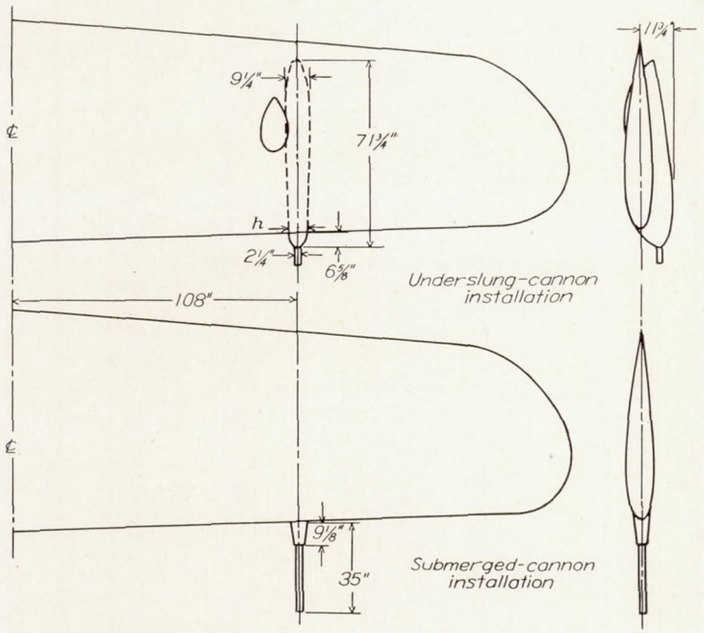

FIGURE 18.—Effect of various 20-millimeter-cannon installations on the maximum lift coefficient of airplane 11.

airplane 11 are given in reference 8. The results of these tests are summarized in figures 17 and 18. The $C_{L_{max}}$ of 2.00 for the airplane with bare wings and landing flaps deflected was used as a reference value for estimating the effects of the various machine-gun and cannon installations.

The smallest reduction in $C_{L_{max}}$ was measured with the machine guns mounted in the flush position (fig. 17). The $C_{L_{max}}$ with four flush guns mounted in the high position (fig. 19) was only slightly lower than the reference value, whereas the $C_{L_{max}}$ was decreased 0.06 below the reference value with the flush guns in the low position (fig. 20). The lowest value of $C_{L_{max}}$ (1.86) was measured with the 2-inch barrel extension (fig. 21). The combination of 10-inch barrel extension and low flush-gun mounting fairings and breech fairings (fig. 22) decreases the $C_{L_{max}}$ by 0.09. With these fairings removed, the $C_{L_{max}}$ was reduced 0.13 below the reference value. The $C_{L_{max}}$ was 1.91 with the 18-inch barrel extension (fig. 23). It is possible that, with the 18-inch extension, the disturbances caused by the ends of the gun barrels passed over the wings and resulted in a smaller loss of $C_{L_{max}}$ than with the 2-inch and 10-inch extensions.

Three 20-millimeter-cannon installations were tested on airplane 11 and included the underslung wing cannon shown as installation 1 (fig. 24), a modification designated cannon installation 2, and the completely submerged installation (fig. 25). The results of these tests (fig. 18) show that the highest $C_{L_{max}}$ (1.96) was measured for the submerged installations. The maximum lift coefficient was 1.91 for underslung installation 1. Installation 1 was then modified to installation 2 by decreasing the width of the section near the leading edge of the wing and thereby reducing the abrupt pressure change at the front of the cannon fairing. The maximum lift coefficient was 1.95 for cannon installation 2.

The effect of installing a 37-millimeter-cannon mock-up at the leading edge of each wing of airplane 4, which has low-drag airfoil sections, is shown in figure 26. Observations were made with the tufts on only the left wing. The results of these tests showed that the cannon installation caused premature wing stall which resulted in a reduction of 0.13 in $C_{L_{max}}$ and of about 3° in the angle of maximum lift. The adverse effects of mounting a cannon on a wing may be reduced by installing a fairing at the wing-cannon juncture to insure smooth air flow over the wing section directly behind the cannon.

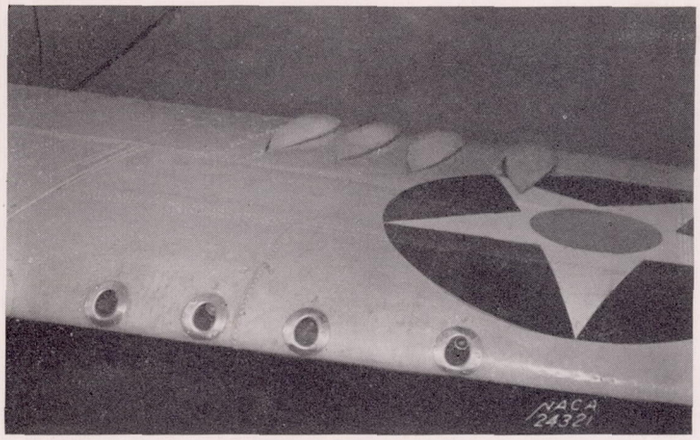

FIGURE 19.—Flush machine guns in high position on left wing. Airplane 11.

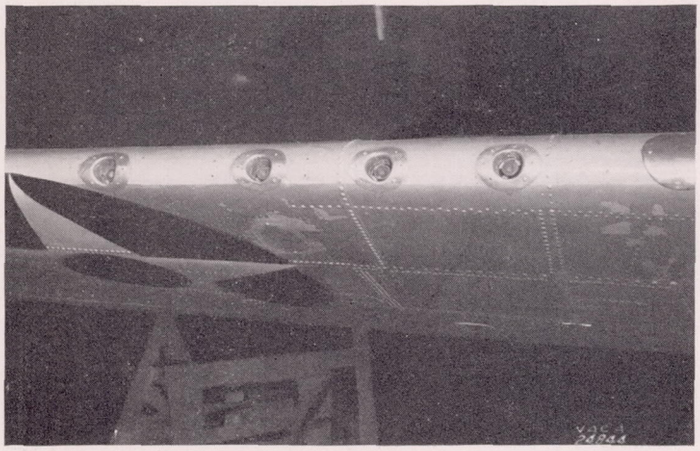

FIGURE 20.—Flush machine guns in low position on right wing. Airplane 11.

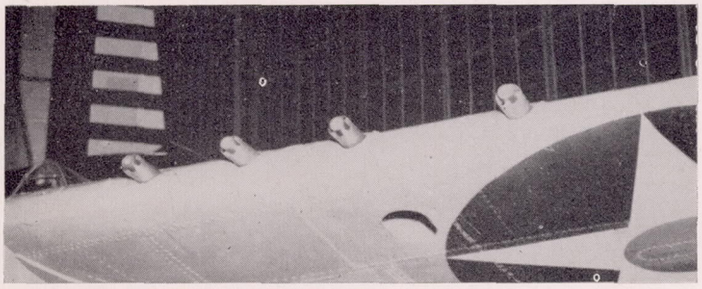

FIGURE 21.—Two-inch barrel extension in high position on left wing. Airplane 11.

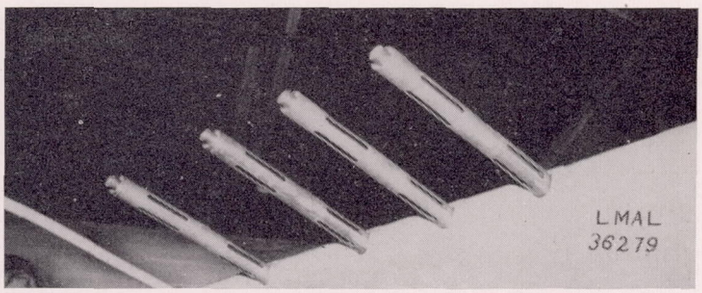

FIGURE 23.—Eighteen-inch barrel extension in low position on right wing. Airplane 11.

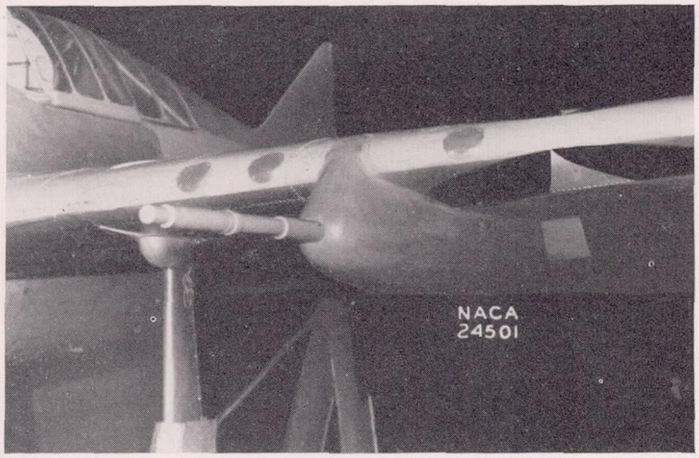

FIGURE 24.—Underslung-cannon installation 1. Airplane 11.

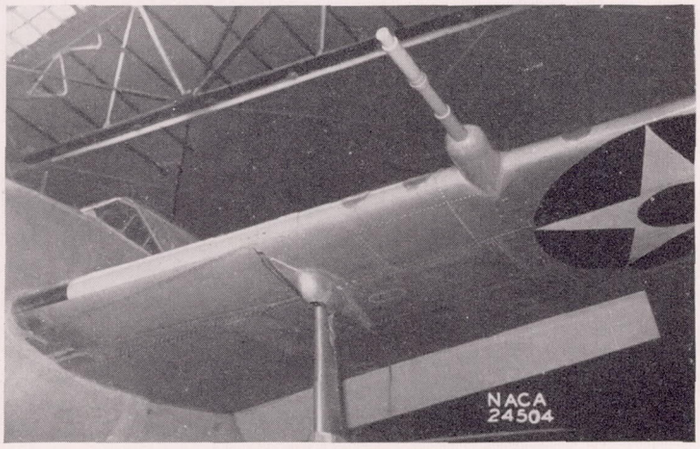

FIGURE 25.—Submerged-cannon installation. Airplane 11.

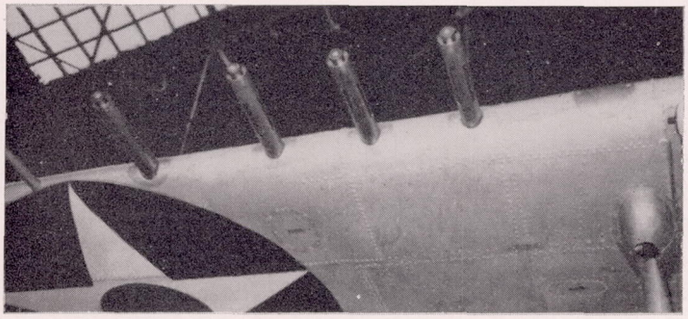

FIGURE 22.—Ten-inch barrel extension in low position on right wing. Airplane 11.

Two mock-ups of 20-millimeter cannon were tested on both wings of airplanes 5, 6, and 1 to determine the effects on $C_{L_{max}}$; the results of these tests and sketches showing the cannon installations are given in figure 27. The largest reduction in $C_{L_{max}}$ due to the cannon installations was measured for airplane 5, which had no fairing at the wing-cannon juncture. For this case, $C_{L_{max}}$ was reduced from 1.77 for the bare wing with flaps deflected to 1.71 for the wing with the four cannon mock-ups installed. The cannon installation on airplane 1, which has a low-drag wing, caused a reduction of only 0.02 in $C_{L_{max}}$. The sketches in figure 27 show clearly that the cannons were faired smoothly into the wing of this airplane so that no abrupt changes occurred at the wing-cannon juncture.

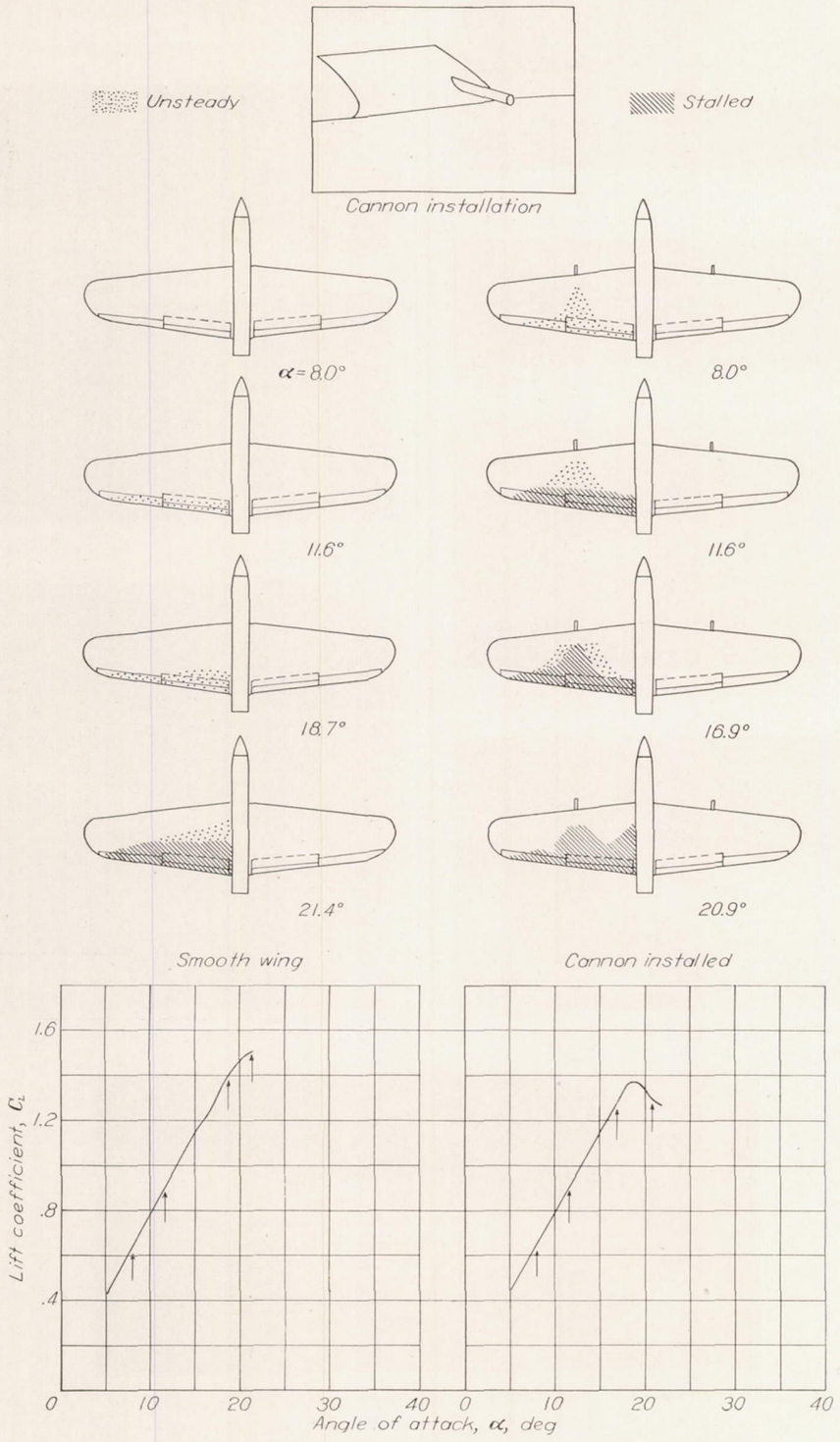

FIGURE 26.—Effect on stall and maximum lift of installing a 37-millimeter-cannon mock-up on the leading edge of the wing of airplane 4. $\delta_f=0°$; approximate test velocity, 60 miles per hour. Tufts on left wing only.

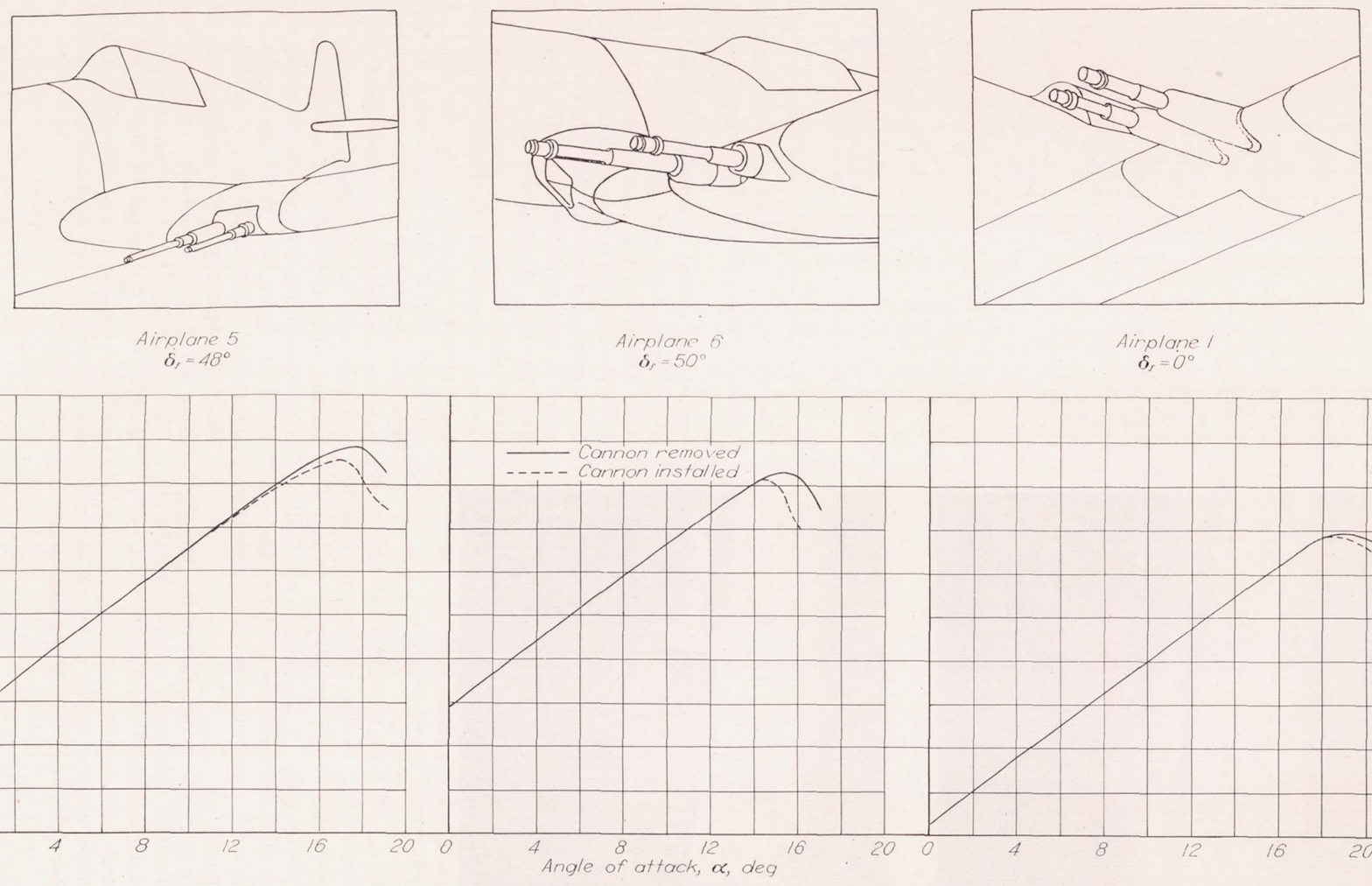

FIGURE 27.—Effect of various cannon installations on the maximum lift coefficients of airplanes 5, 6, and 1. Cannon installed on both wings.

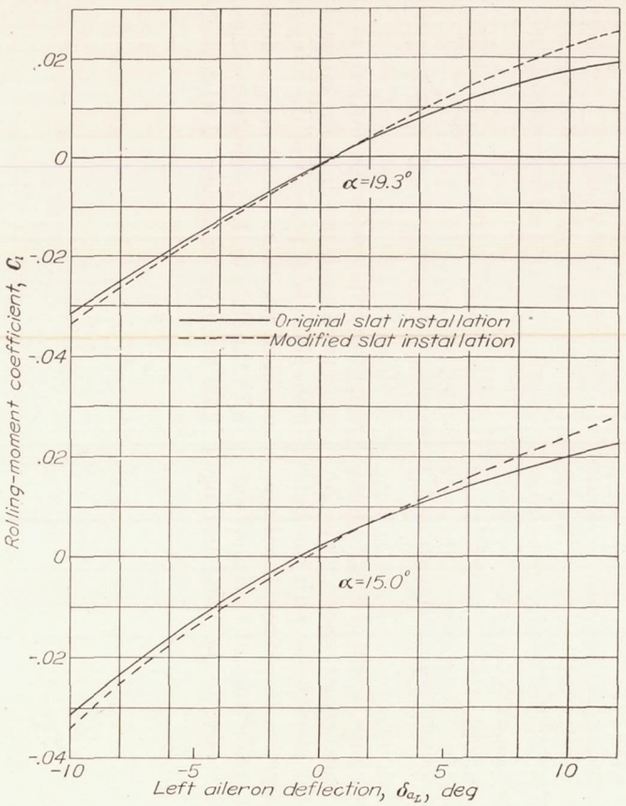

FIGURE 31.—Effect of slat installation on the aileron control characteristics of airplane 7. Both ailerons deflected; δ_f=60°.

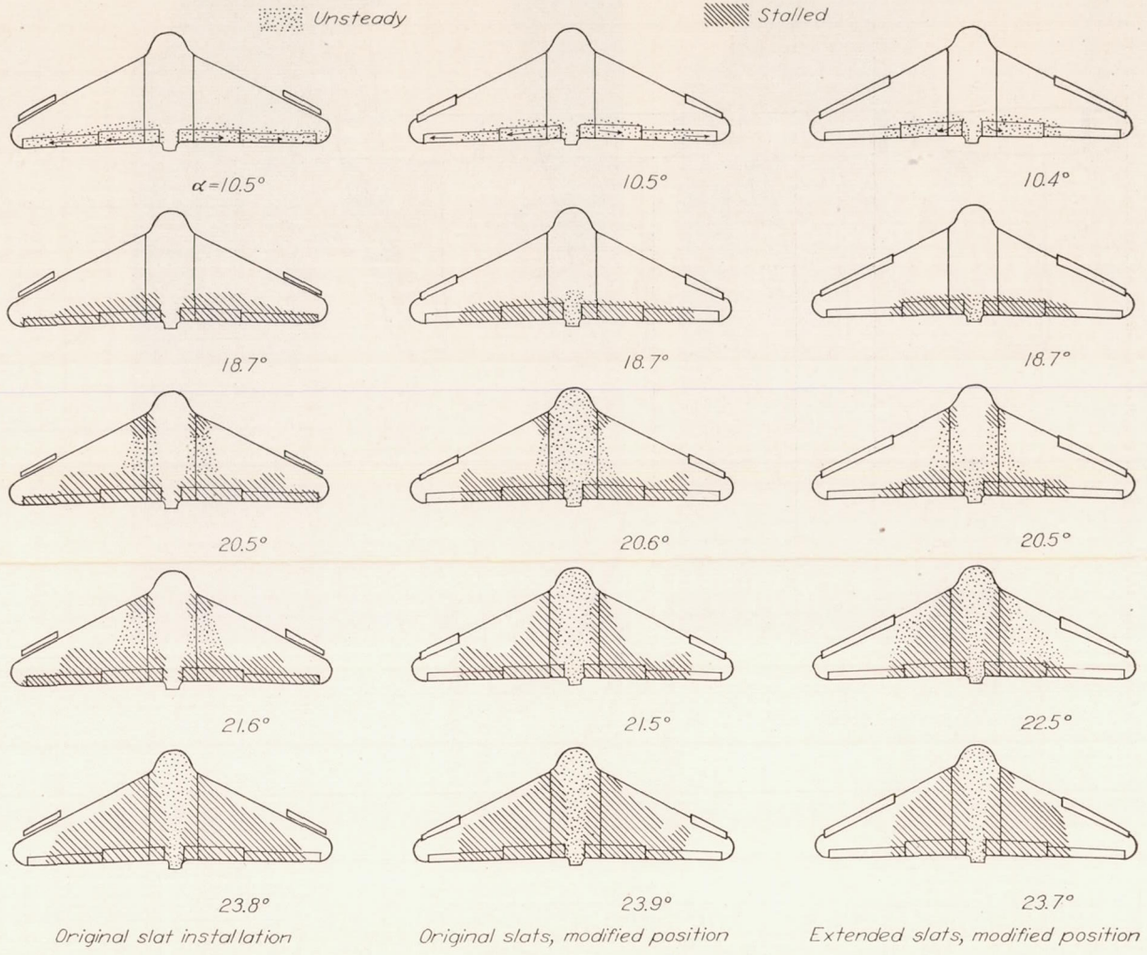

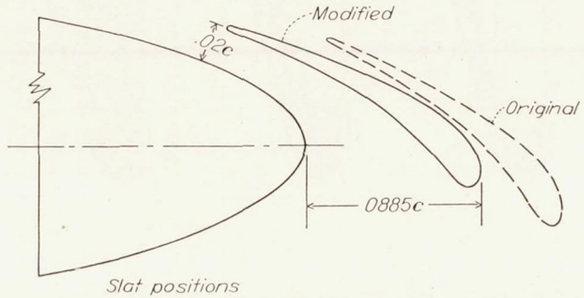

FIGURE 32.—Effect of slat length and position on the stall progression of airplane 9. Control surfaces neutral; approximate test velocity, 60 miles per hour.

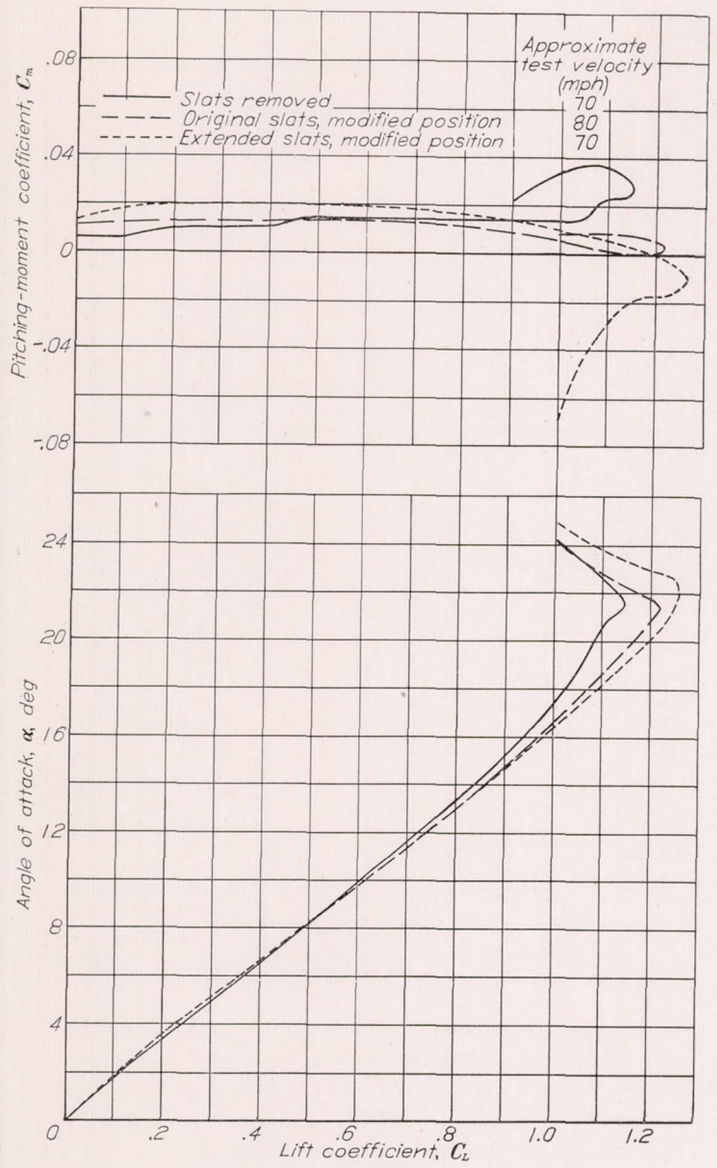

FIGURE 33.—Effect of slat length and position on the variation of C_m and α with lift coefficient for airplane 9.

modified slats. Stall progressions for the airplane with the slats removed are given in figure 5. The results of the stall studies show that each slat modification successively improved the air flow over the outer sections of the wing.

The effects of the slat modifications on the variation of C_m with C_L and on the $C_{L_{max}}$ of airplane 9 are shown in figure 33. The extended slats in the modified position eliminated the longitudinal instability near the stall and in addition increased the maximum lift coefficient to 1.26 from 1.15 for the airplane with the slats removed. Although the tests with the original slats in the modified position were made at a slightly higher tunnel speed, it is fairly evident that this slat installation decreased the longitudinal instability at high lift coefficients and also increased the maximum lift coefficient of the airplane.

Wing ducts.—Considerable difficulty is usually encountered in the design of the shape and location of wing-duct inlets owing to the critical nature of the flow at the leading edge of a wing. In general, if the inlet is placed too high on the wing leading edge, the internal flow separates from the lower lip of the duct inlet at moderate angles of attack whereas the external flow separates over the upper lip of the duct inlet at high angles of attack and thereby induces a premature stall and a low value of $C_{L_{max}}$. If the inlet is placed too low, the external flow separates at low angles of attack from the upper lip just within the inlet and thus causes serious losses of total pressure.

A study of several ducts installed in the wings of a full-scale mock-up of a conventional single-engine pursuit airplane (airplane 16) was made in the Langley full-scale tunnel to determine the influence of inlet design on the pressure losses within the duct and on the aerodynamic characteristics of the airplane. The results of some of these tests, which are reported in reference 9, are given in figures 34 to 36. The inlet profiles, which are shown in figures 34 and 36, are numbered in accordance with the inlet designations given in reference 9. The effect of inlet size and shape on the maximum lift coefficient of the airplane is shown in figure 34 and the effect of lift coefficient on the average total pressure at the front of the radiator behind these same three inlets is given in figure 35. Inasmuch as the inlet areas were not equal for all the ducts, the inlet-velocity ratios were unequal at any particular lift coefficient; it is believed, however, that this difference will not detract from the general conclusions drawn from the results. The highest $C_{L_{max}}$ was obtained with inlet 5 installed on both wings, but the total-pressure recovery at the heat exchanger behind this inlet dropped off very rapidly above a lift coefficient of 0.4. For this inlet, the diffuser and the plane of the inlet opening were inclined farther downward from the wing chord line than for inlets 2 and 4. Inlet 4 gave the best over-all total-pressure recovery at the heat exchanger; the maximum lift coefficient with this inlet installed on both wings, however, was 0.07 lower than for inlet 5. The lowest $C_{L_{max}}$ and over-all total-pressure recovery was measured for inlet 2, for which the diffuser and the plane of the inlet opening were most nearly parallel and perpendicular, respectively, to the wing chord line. Reference 9 shows that, of the inlets tested, the one giving the best compromise between high pressure recoveries at the heat exchanger and satisfactory maximum-lift characteristics of the ducted wing had an upper lip with a large leading-edge radius conforming approximately to the contour of the original wing, a lower lip cut back to turn the inlet plane downward 70° to the chord line, and a diffuser inclined approximately 10° to the wing chord line.

Stall progressions and lift data are given in figure 36 for three very dissimilar duct inlets located in the left wing of airplane 16. These results further emphasize the effects on maximum lift coefficient of lip position, leading-edge radius, and diffuser inclination. The highest $C_{L_{max}}$ (1.37) was obtained for inlet 7, which has the diffuser inclined downward 11° to the chord line and a large upper-lip leading-edge radius. The maximum lift coefficient was only 1.26 for inlet 1, for which the plane of the inlet opening was perpendicular to the wing chord line. Inlet 6 was fitted with a flapped lower lip that could be adjusted to provide smooth entry of the air flow into the duct over a wide range of angle of attack; for this case, however, the $C_{L_{max}}$ was still low (1.22), probably because of the sharp leading-edge radius of the upper lip.

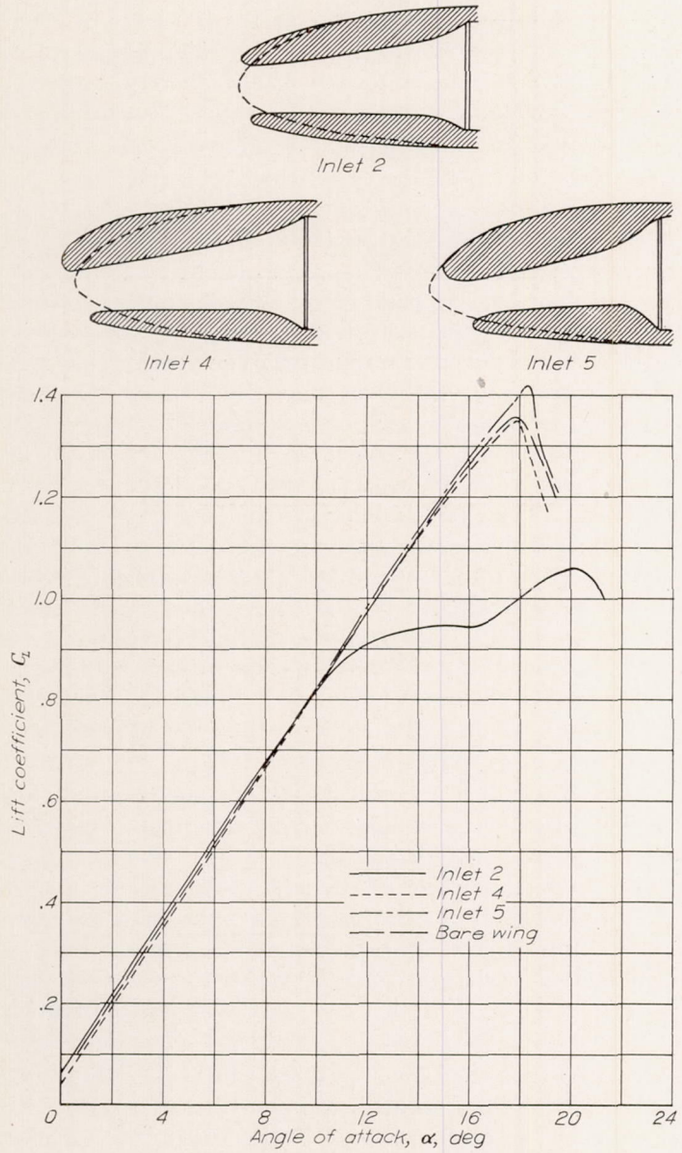

FIGURE 34.—Effect of inlet size and shape on the maximum lift coefficient of airplane 16. Propeller removed; $\delta_f=0°$; bottom outlet. Inlets installed on both wings.

The effects of the location of wing-duct outlets on the maximum lift and stall of airplane 16 are shown in figure 37. The maximum lift coefficient of the airplane was 0.07 less with the outlet at the bottom of the wing than with the outlet at the top of the wing. A wing-duct outlet located on the upper surface of a wing has an advantage over a bottom outlet, other than giving a higher maximum lift coefficient, inasmuch as the quantity of air flowing through the duct automatically tends to be adjusted with angle of attack because of the relative increase with lift coefficient of the negative pressure at the outlet.

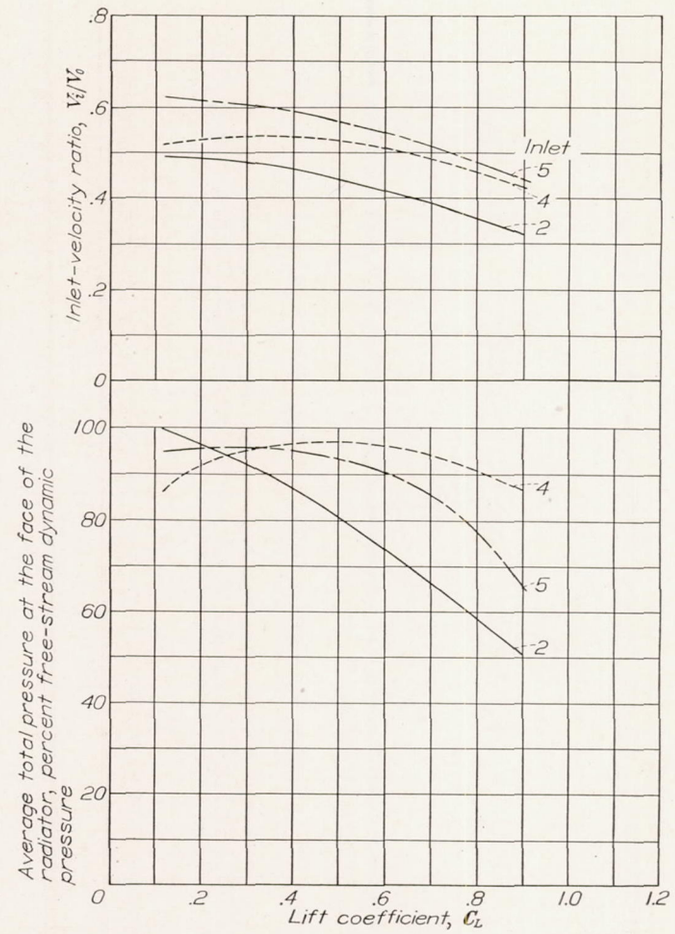

FIGURE 35.—Effect of lift coefficient on the average total pressure at the front of the radiator behind inlets 2, 4, and 5. Propeller removed; $\delta_f=0°$; bottom outlet; airplane 16.

Total-pressure measurements in the wing ducts of airplane 2 with propeller operating showed that the flow separated from the lower lip of the inlet of the left duct, especially in the climbing condition. This separation was probably due to the slipstream rotation, which increased the effective angle of attack at the left duct inlet behind the upgoing propeller blades. In addition, the inlet-velocity ratios were too high and caused separation of the internal flow. In order to remedy these difficulties, the inlet areas of both ducts were increased and the plane of the inlet opening of the left duct was increased from 14° to 29° as shown in figure 38. The effects of these modifications on the maximum lift coefficient of the airplane with the propeller removed and with landing flaps and duct exit flaps retracted and deflected are also shown in figure 38. With the landing flaps and duct exit flaps retracted, the $C_{L_{max}}$ was increased from 1.10 for the original duct installation to 1.26 for the modified ducts. With the landing flaps extended 45° and duct exit flaps deflected 41°, the $C_{L_{max}}$ was increased from 1.30 to 1.43.

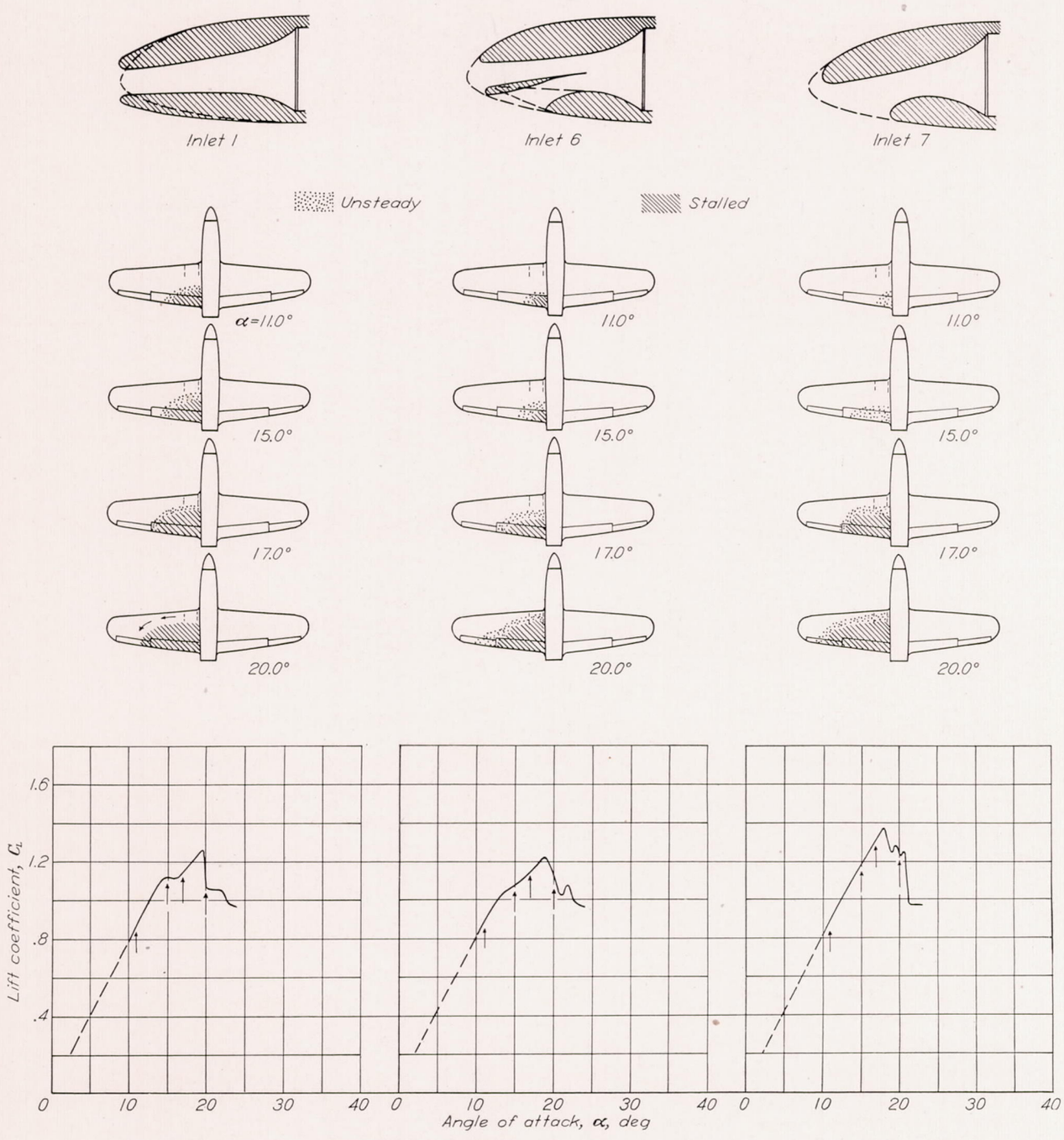

FIGURE 36.—Effect of wing-duct-inlet shape on the stalling characteristics of airplane 16. Inlet and tufts on left wing only. Propeller removed: $\delta_f=0°$; approximate test velocity, 60 miles per hour. Outlet at bottom of wing.

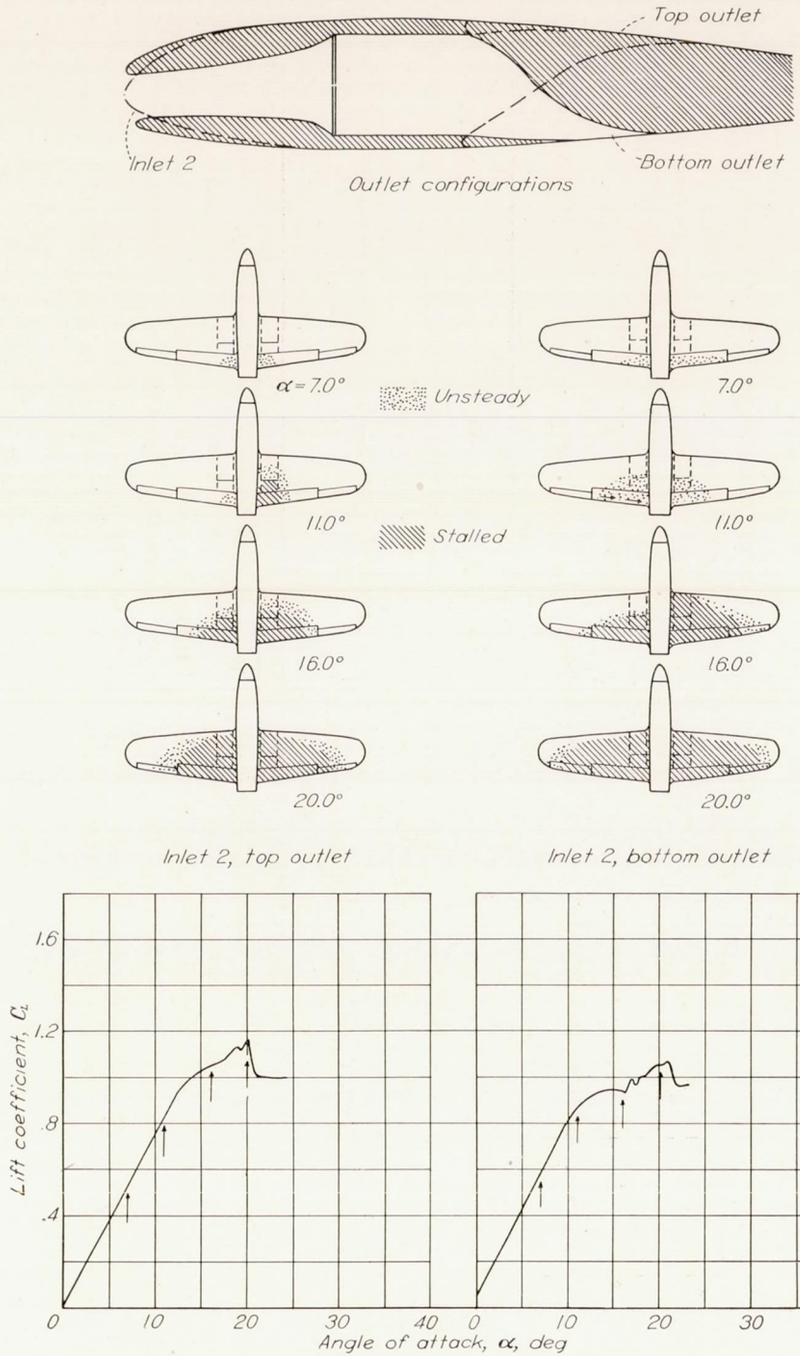

FIGURE 37.—Effect of wing-duct-outlet location on the stalling characteristics of airplane 16. Propeller removed; δ_f=0°; approximate test velocity, 60 miles per hour.

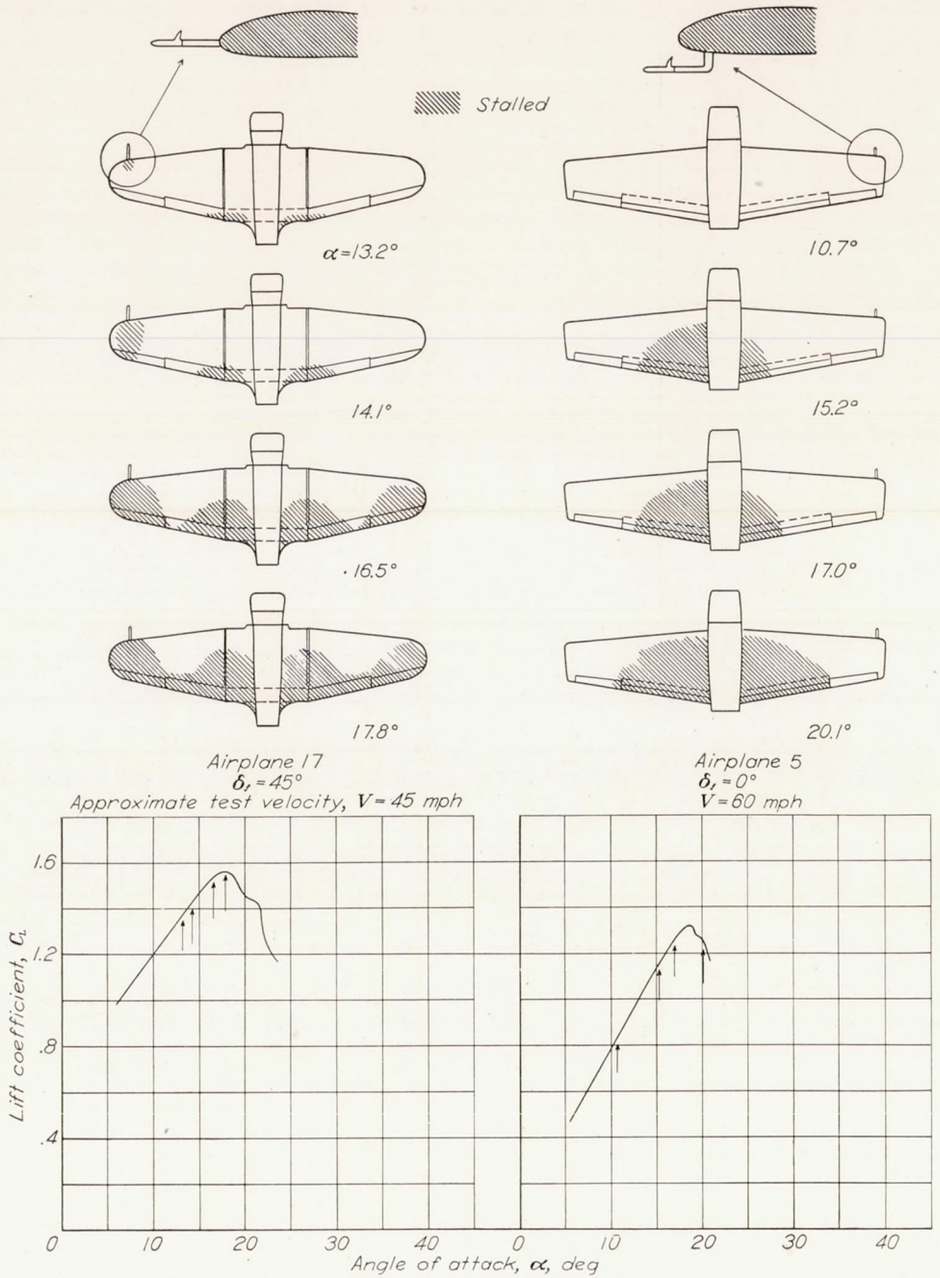

FIGURE 39.—Effect of airspeed-head location on stalling characteristics. Propellers removed.

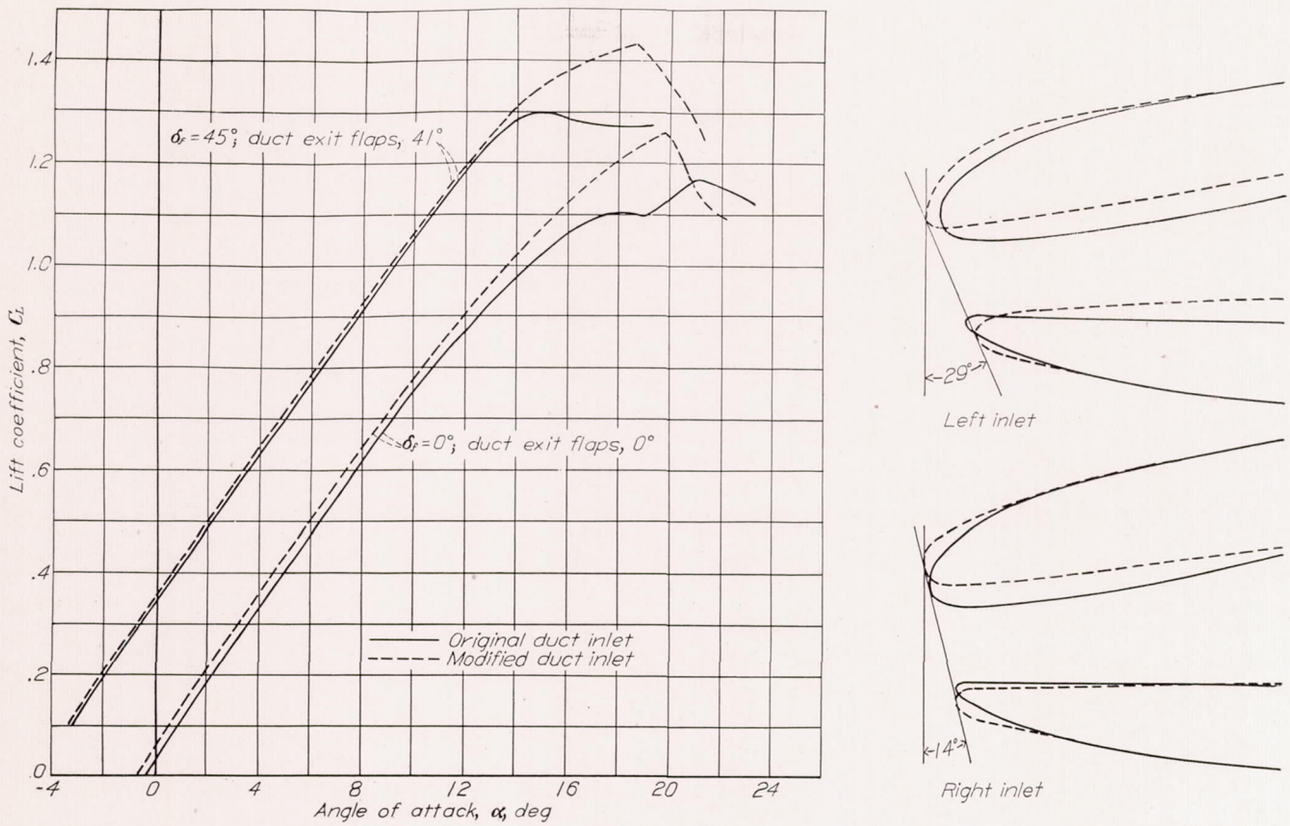

FIGURE 38.—Effect of duct-inlet modifications on the $C_{L_{max}}$ of airplane 2. Propeller removed; wing guns installed; approximate test velocity, 60 miles per hour.

Airspeed heads.—The effect on the air flow over the wings of placing airspeed heads at the leading edges of the wings of two airplanes (airplanes 17 and 5) is shown in figure 39. The airspeed head on airplane 17 was located directly at the wing leading edge and resulted in a premature stall over the section of the wing behind the head. No effect on the flow over the wing was observed for the airspeed-head installation on airplane 5. This airspeed head was located on the lower surface of the wing and extended forward below the wing leading edge.

COMPARISON OF SPLIT AND SLOTTED FLAPS

An analysis was made of the increments of lift coefficient contributed by split and slotted flaps when installed on airplanes to ascertain whether these values could be predicted from results of tests in two-dimensional flow. Measured values of ΔC_{L_f} obtained from tests of flaps installed on the airplanes and corresponding values of ΔC_{L_f} computed from available two-dimensional data for similar flaps installed on smooth wings are compared in figures 40 and 41. The lift increments due to the flaps have been taken at about 3° below the stalling angle of the wing with flaps retracted or deflected (whichever gave the lower values), inasmuch as these values have been found to be relatively independent of test conditions such as Reynolds number and wind-tunnel turbulence (reference 10). For comparison, the two-dimensional lift data have been evaluated for partial-span flaps by the methods presented in reference 11.

The measured values of ΔC_{L_f} for the split-flap installations showed good agreement in every case with the values computed from two-dimensional data. For the slotted-flap installations, however, the measured values were, on the average, about 20 percent lower than the calculated values. The reason for the low values of ΔC_{L_f} obtained for the slotted-flap installations is probably the difficulties encountered by manufacturers in producing slot shapes of efficient aerodynamic design. Tests of an NACA 23012 airfoil equipped with various arrangements of slotted flaps (reference 12) showed that, in order to obtain high lift increments, the nose of the flap should be located slightly ahead of and below a slot lip that directs the air downward over the flap. In addition, in order to obtain low values of drag at moderate lift coefficients, the nose of the flap should have a good aerodynamic form and the slot entry should be of such shape that no abrupt changes in the air-flow direction occur.

COMPARISON OF FULL-SCALE-TUNNEL AND FLIGHT MEASUREMENTS OF $C_{L_{max}}$

In order to compare wind-tunnel and flight measurements of the maximum lift coefficient of an airplane, several factors must be considered. Previous investigations (references 13 and 14) have shown that the maximum lift coefficients obtained in tests with changing angle of attack were considerably higher than those obtained in tests in which the forces were measured with the angle of attack fixed. The difference is attributed to the lag in the separation tendency with changing angle of attack.

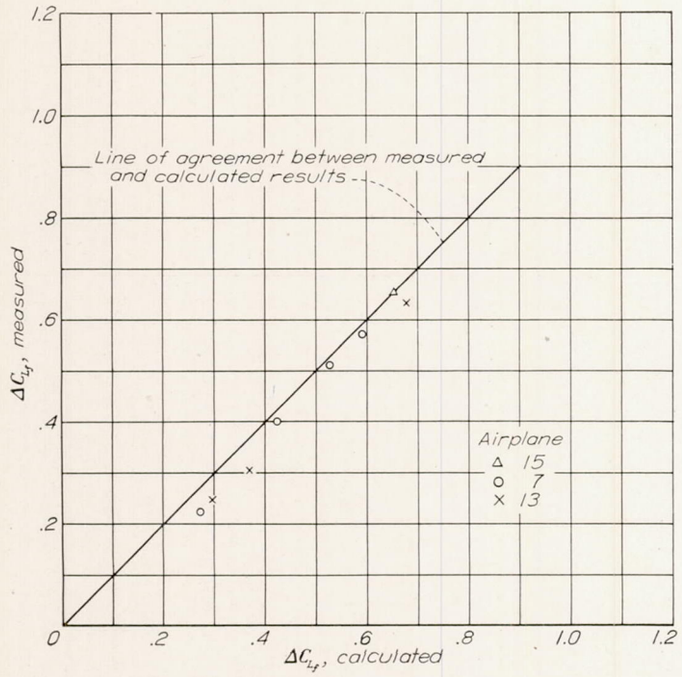

FIGURE 40.—Comparison between measured and calculated values of the increments in lift coefficient due to flap deflection. Split flaps.

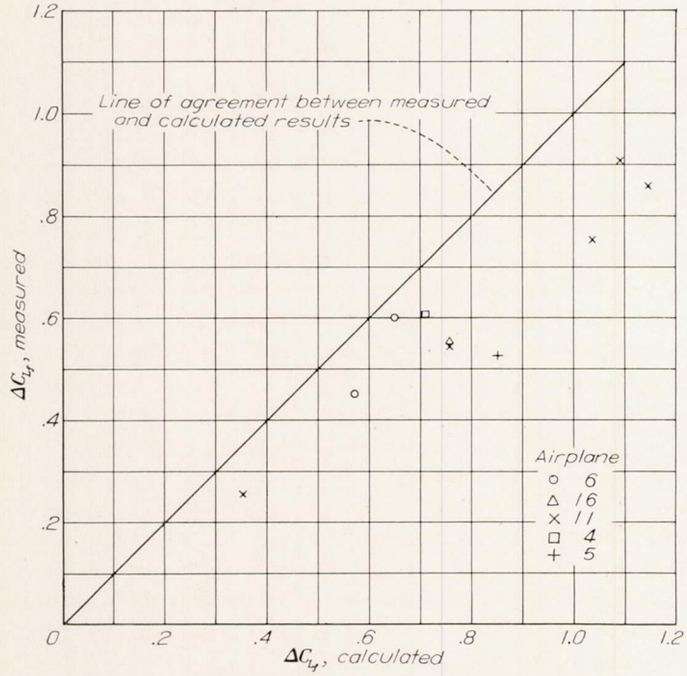

FIGURE 41.—Comparison between measured and calculated values of the increments in lift coefficient due to flap deflection. Slotted flaps.

Maximum lift coefficients obtained in flight and in wind tunnels should be compared at the same Reynolds number. For the normal range of full-scale-tunnel and flight Reynolds numbers, the maximum lift coefficients will increase with Reynolds number. In order to show the magnitude of the Reynolds number effect, the variation of $C_{L_{max}}$ with Reynolds number has been plotted in figure 42 for several of the airplanes (airplanes 18, 13, 4, and 16) and for an NACA 23012 wing. Except for the case of airplane 4, the $C_{L_{max}}$ increased about 0.10 for each increase of 1×10^6 in Reynolds number. For airplane 4, which has a wing with low-drag airfoil sections (NACA 66 series), the increase in $C_{L_{max}}$ with Reynolds number was considerably greater.

Propeller operation, even with idling power applied, may also appreciably increase the $C_{L_{max}}$ of an airplane over that measured with the propeller removed. In comparing wind-tunnel and flight measurements of $C_{L_{max}}$, conditions of propeller operation must therefore be reproduced. The effect of idling propellers on the maximum lift coefficient of two typical present-day airplanes (airplanes 5 and 2) is shown in figure 43. The measurements were made in the wind tunnel by completely closing the engine throttles and measuring the forces with the engine idling. Increases of 0.13 and 0.08 in $C_{L_{max}}$ due to the idling propellers were measured for airplanes 5 and 2, respectively.

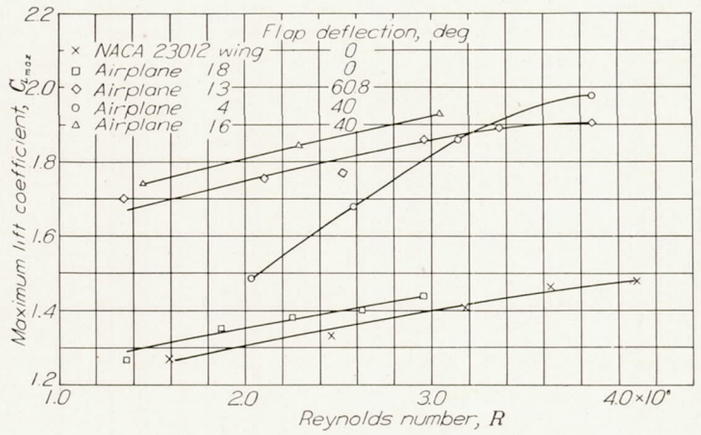

FIGURE 42.—Effect of Reynolds number on the maximum lift coefficient of several airplanes and an NACA 23012 wing tested in the Langley full-scale tunnel.

Full-scale-tunnel and flight determinations of the maximum lift coefficient of an airplane have been shown to be in agreement when tests were made under similar test conditions of Reynolds number, slipstream, and time rate of change of angle of attack $d\alpha/dt$. As an example, reference is made to comparative flight and full-scale-tunnel measurements of the $C_{L_{max}}$ of airplane 18 (reference 13). Special care was taken in this case to reproduce the flight test conditions in the wind tunnel and the results of the measurements showed agreement within 3 percent.

The maximum lift coefficients of airplane 11 as determined for several flap deflections from full-scale-tunnel and flight tests are compared in figure 44. The large discrepancies between the two sets of measurements are attributed, in this case, to differences in the testing techniques. An analysis of the flight-test records showed that these measurements were made at values of $d\alpha/dt$ varying from 0.2° to 1.0° per second; the full-scale-tunnel measurements were made with the angle of attack fixed. The full-scale-tunnel measurements, in addition, were made with the propeller removed from the airplane; and the test Reynolds numbers for the full-scale-tunnel measurements were between 0.5×10^6 and 1×10^6 less than the flight test Reynolds

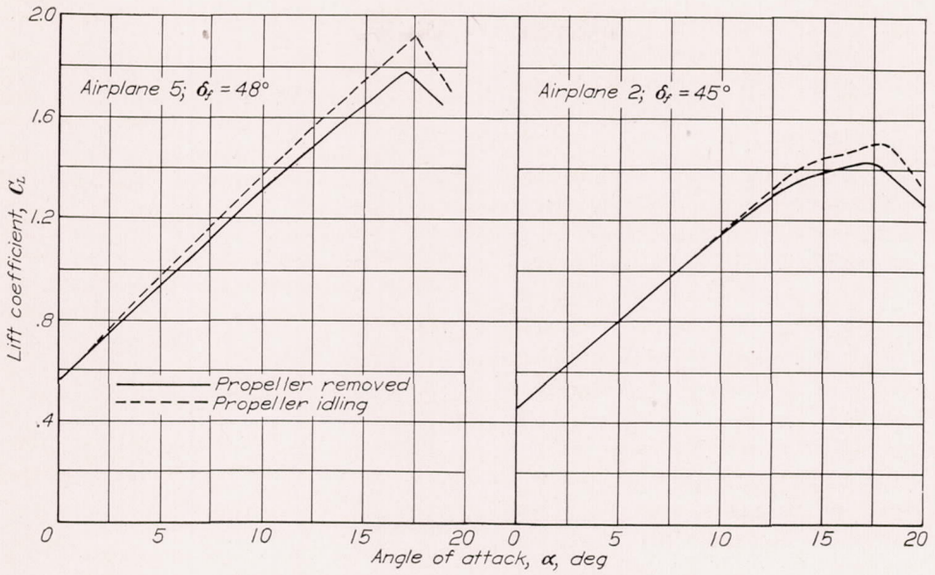

FIGURE 43.—Effect of idling propellers on the maximum lift coefficient of two present-day airplanes. Approximate test velocity, 60 miles per hour.

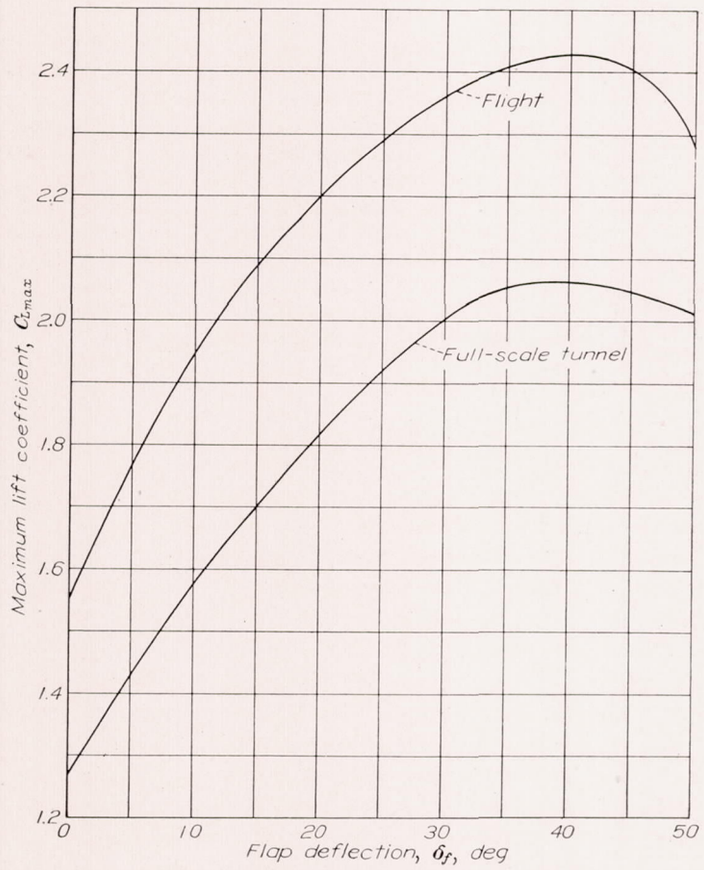

FIGURE 44.—Comparison between flight and full-scale-tunnel measurements of the maximum lift coefficient of airplane 11. Full-span flaps.

numbers. The exact contribution to $C_{L_{max}}$ of the propeller, of $d\alpha/dt$, and of the variation in Reynolds number is not readily estimable at present because of the lack of sufficient theoretical or experimental data; some rough approximations, however, indicated that the combined effects of propeller operation, $d\alpha/dt$, and Reynolds number may account for the discrepancies shown in figure 44.

CONCLUSIONS

From the results of maximum-lift and stall measurements of 18 airplanes tested in the Langley full-scale tunnel, the following conclusions were drawn:

1. Large improvements in the stalling characteristics and maximum lift coefficients of airplanes can be obtained by careful attention to detail design.

2. Wings having high taper ratios and large amounts of sweepback have been shown to be subject to poor stalling characteristics because they are susceptible to tip stalling. The proper combinations of washout and changes in camber and wing thickness from root to tip with taper will usually produce satisfactory stalls on wings subject to tip stalling.

3. The addition of fuselages and nacelles to wings frequently introduces centers of local separation and may reduce the maximum lift coefficient if the wing-fuselage or wing-nacelle junctures are not adequately faired.

4. Deflection of the landing flaps generally tended to "clean up" the inboard sections of a wing and increased the upwash over the outer unflapped portions of the wing.

5. Propeller operation will generally increase the severity of the stall, especially on single-engine airplanes, by producing an asymmetrical stall pattern and by cleaning up the inboard sections of the wings.

6. The maximum lift coefficient of an airplane may be appreciably increased by the elimination of wing surface roughness and air leakage through the wings.

7. The detrimental effects of placing machine guns and cannon at the leading edge of a wing may be reduced considerably by properly locating the guns in the wings. Highest maximum lift coefficients were measured for machine-gun installations in which the ends of the barrels were flush with the wing surface at the leading edge and slightly above the wing chord line and for cannon installations that were submerged in the wings.

8. Wing-duct inlets with well-cambered upper lips properly alined with the flow at the leading edge of the wing will

generally cause no reduction in the maximum lift coefficient of an airplane; whereas substantial decreases in the maximum lift coefficient of an airplane may be caused by ducts with the inlet plane perpendicular to the chord line and by inlet lips with small leading-edge radii.

9. The increments of lift coefficient contributed by split flaps could be computed with sufficient accuracy by the use of two-dimensional test data; for slotted flaps, however, the measured increments of lift coefficient were, on the average about 20 percent lower than those calculated from the available two-dimensional test data. These low values for the slotted flaps are attributed, mainly, to difficulties encountered by manufacturers in producing slot shapes of efficient aerodynamic design.

10. In a single instance where great care was taken to reproduce the test conditions of Reynolds number, propeller operation, and the time rate of change of angle of attack, satisfactory agreement of the maximum lift coefficients determined from full-scale-tunnel and flight tests was obtained. It is believed that equally satisfactory agreement may be obtained with other airplanes provided that sufficient care is taken to reproduce the test conditions.

LANGLEY MEMORIAL AERONAUTICAL LABORATORY,
NATIONAL ADVISORY COMMITTEE FOR AERONAUTICS,
LANGLEY FIELD, VA., *May 19, 1944.*

REFERENCES

1. DeFrance, Smith J.: The N.A.C.A. Full-Scale Wind Tunnel. NACA Rep. No. 459, 1933.
2. Anderson, Raymond F.: Determination of the Characteristics of Tapered Wings. NACA Rep. No. 572, 1936.
3. Anderson, Raymond F.: The Experimental and Calculated Characteristics of 22 Tapered Wings. NACA Rep. No. 627, 1938.
4. Soulé, H. A., and Anderson, R. F.: Design Charts Relating to the Stalling of Tapered Wings. NACA Rep. No. 703, 1940.
5. Young, A. D.: A Review of Recent Stalling Research. Rep. No. Aero 1718, British R. A. E., March 1942.
6. Annand, W. J. D.: Further Notes on the Stalling Characteristics of Monoplanes. Rep. No. A. & A. E. E./Res/164 (rev.) (British), Nov. 18, 1942.
7. Mutterperl, William: The Calculation of Span Load Distributions on Swept-Back Wings. NACA TN No. 834, 1941.
8. Quinn, John H., Jr.: Summary of Data Relating to the Effects of Wing Machine-Gun and Cannon Installations on the Aerodynamic Characteristics of Airplanes. NACA ACR No. L4L21, 1945.
9. Nelson, W. J., and Czarnecki, K. R.: Wind-Tunnel Investigation of Wing Ducts on a Single-Engine Pursuit Airplane. NACA ARR No. 3J13, 1943.
10. Young, A. D., and Hufton, P. A.: Note on the Lift and Profile Drag Effects of Split and Slotted Flaps. Rep. No. B. A. 1707, British R. A. E., Sept. 1941.
11. Silverstein, Abe, and Katzoff, S.: Design Charts for Predicting Downwash Angles and Wake Characteristics behind Plain and Flapped Wings. NACA Rep. No. 648, 1939.
12. Wenzinger, Carl J., and Harris, Thomas A.: Wind-Tunnel Investigation of an N. A. C. A. 23012 Airfoil with Various Arrangements of Slotted Flaps. NACA Rep. No. 664, 1939.
13. Silverstein, Abe, Katzoff, S., and Hootman, James A.: Comparative Flight and Full-Scale Wind-Tunnel Measurements of the Maximum Lift of an Airplane. NACA Rep. No. 618, 1938.
14. Farren, W. S.: The Reaction on a Wing Whose Angle of Incidence is Changing Rapidly. Wind Tunnel Experiments with a Short Period Recording Balance. R. & M. No. 1648, British A. R. C., 1935.
15. Abbott, Ira H., Von Doenhoff, Albert E., and Stivers, Louis S., Jr., Summary of Airfoil Data. NACA Rep. No. 824, 1945.

U. S. GOVERNMENT PRINTING OFFICE: 1949

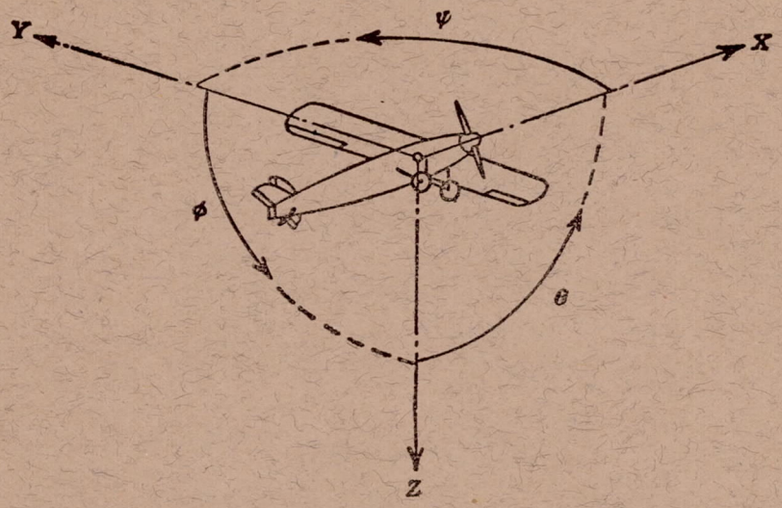

Positive directions of axes and angles (forces and moments) are shown by arrows

Axis		Force (parallel to axis) symbol	Moment about axis			Angle		Velocities	
Designation	Symbol		Designation	Symbol	Positive direction	Designation	Symbol	Linear (component along axis)	Angular
Longitudinal	X	X	Rolling	L	$Y \longrightarrow Z$	Roll	ϕ	u	p
Lateral	Y	Y	Pitching	M	$Z \longrightarrow X$	Pitch	θ	v	q
Normal	Z	Z	Yawing	N	$X \longrightarrow Y$	Yaw	ψ	w	r

Absolute coefficients of moment

$C_l = \frac{L}{qbS}$ (rolling) $\quad C_m = \frac{M}{qcS}$ (pitching) $\quad C_n = \frac{N}{qbS}$ (yawing)

Angle of set of control surface (relative to neutral position), δ. (Indicate surface by proper subscript.)

4. PROPELLER SYMBOLS

D Diameter

p Geometric pitch

p/D Pitch ratio

V' Inflow velocity

V_s Slipstream velocity

T Thrust, absolute coefficient $C_T = \frac{T}{\rho n^2 D^4}$

Q Torque, absolute coefficient $C_Q = \frac{Q}{\rho n^2 D^5}$

P Power, absolute coefficient $C_P = \frac{P}{\rho n^3 D^5}$

C_s Speed-power coefficient $= \sqrt[5]{\frac{\rho V^5}{P n^2}}$

η Efficiency

n Revolutions per second, rps

Φ Effective helix angle $= \tan^{-1}\left(\frac{V}{2\pi r n}\right)$

5. NUMERICAL RELATIONS

1 hp=76.04 kg-m/s=550 ft-lb/sec

1 metric horsepower=0.9863 hp

1 mph=0.4470 mps

1 mps=2.2369 mph

1 lb=0.4536 kg

1 kg=2.2046 lb

1 mi=1,609.35 m=5,280 ft

1 m=3.2808 ft